MDPI

Article

The Solar Particle Acceleration Radiation and Kinetics (SPARK) mission concept

Hamish A. S. Reid[1,*], Sophie Musset [2], Daniel Ryan[3], Ariadna Calcines Rosario[14], Jaroslav Dudík[JD], Frédéric Auchère[5], Joel Dahlin[6], Laura A. Hayes[2], Graham S. Kerr[X,Y], Valery M. Nakariakov[7], Astrid M. Veronig[8*], Robertus Erdélyi[9,10,11], Philippa Browning[12], Iain Hannah[13], Alexander Warmuth[15], Carsten Denker[15], Meetu Verma[15], Christian Vocks[15], Vanessa Polito[16,17], Vincenzo Andretta[N], Luca Teriaca[T], David M. Long[Q], Giulio Del Zanna[G], Paolo Romano[P], Andrew R. Inglis[X,Y], Steven D. Christe[X], Andrzej Fludra[18], Alain Jody Corso[C], David Orozco Suárez[19,20], Melissa Pesce-Rollins[21], Eduard P. Kontar[22], Lucie M. Green[1], Natasha L. S. Jeffrey[23], Marek Stęślicki[24], Lyndsay Fletcher[22,25], Tomasz Mrozek[24], Säm Krucker[3,26], Nicole Vilmer[27], Albert Y. Shih[6], Éric Buchlin[5], Shane A. Maloney[28], Jana Kašparová[JD], Timo Laitinen[29], Mykola Gordovskyy[30], Christian Kintziger[31], Richard Harrison[32], Olivier Limousin[33], Philippe Laurent[33], Michele Piana[34,36], Anna Maria Massone[34], Federico Benvenuto[34], Paolo Massa[35], Sarah Matthews[1], Clementina Sasso[N], Silvia Dalla[29], Salvo L. Guglielmino[P], Ilaria Ermolli[37]

[1] University College London, Mullard Space Science Laboratory, Holmbury Hill Rd, Dorking RH5 6NT
[2] European Space Research and Technology Centre, Noordwijk, Netherlands
[3] University of Applied Sciences and Arts Northwestern Switzerland, Bahnhofstrasse 6, Windisch 5210, Switzerland
[JD] Astronomical Institute of the Czech Academy of Sciences, Fričova 298, 251 65 Ondřejov, Czech republic
[5] Université Paris-Saclay, CNRS, Institut d'Astrophysique Spatiale, 91405, Orsay, France
[6] Astronomy Department, University of Maryland, College Park, MD 20740, USA
[7] Physics Department, University of Warwick, Coventry CV4 7AL, UK
[8] Institute of Physics & Kanzelhöhe Observatory for Solar and Environmental Research, University of Graz, 8010 Graz, Austria
[9] Solar Physics & Space Plasma Research Center (SP2RC), School of Mathematics and Statistics, University of Sheffield, Hounsfield Road, Sheffield, S3 7RH, UK; robertus@sheffield.ac.uk
[10] Department of Astronomy, Eötvös Loránd University, Pázmány Péter sétány 1/A, Budapest H-1117, Hungary
[11] Gyula Bay Zoltan Solar Observatory (GSO), Hungarian Solar Physics Foundation (HSPF), Petőfi tér 3., Gyula H-5700, Hungary.
[12] Jodrell Bank Centre for Astrophysics, University of Manchester, Manchester M13 9PL, UK
[13] School of Physics and Astronomy, University of Glasgow, Glasgow, G12 8QQ, UK
[14] Durham University, Centre for Advanced Instrumentation, Durham, UK
[15] Leibniz-Institut für Astrophysik Potsdam (AIP), An der Sternwarte 16, 14482 Potsdam, Germany
[16] Lockheed Martin Solar and Astrophysics Laboratory, Building 252, 3251 Hanover Street, Palo Alto, CA 94304, USA
[17] Department of Physics, Oregon State University, Corvallis, OR, USA
[18] RAL Space, UKRI STFC, Chilton, Didcot, OX11 0QX, UK
[19] Instituto de Astrofísica de Andalucía (IAA-CSIC), Granada, Spain
[20] Spanish Space Solar Physics Consortium (S^3PC)
[X] NASA Goddard Space Flight Center, Heliophysics Science Division, Code 671, Greenbelt, MD 20771, USA
[Y] Department of Physics, Catholic University of America, Washington DC 20064, USA
[N] INAF / Capodimonte Astronomical Observatory, 80131 Naples, Italy
[T] Max Planck Institute for Solar System Research, 37077 Göttingen, Germany
[Q] Astrophysics Research Centre, School of Mathematics and Physics, Queen's University Belfast, University Road, Belfast, BT7 1NN, Northern Ireland, UK
[G] DAMTP, Centre for Mathematical Sciences, University of Cambridge, Wilberforce Road, Cambridge CB3 0WA, UK
[C] National Research Council of Italy, Institute for Photonics and Nanotechnologies, via Trasea 7, 35131, Padova, Italy
[P] INAF – Catania Astrophysical Observatory, 95123 Catania, Italy
[21] Istituto Nazionale di Fisica Nucleare, Sezione di Pisa I-56127 Pisa, Italy
[22] University of Glasgow, Glasgow G12 8QQ, UK
[23] Department of Mathematics, Physics & Electrical Engineering, Northumbria University, Newcastle upon Tyne, UK, NE1 8ST
[24] Centrum Badań Kosmicznych PAN, Bartycka 18A, 00-716 Warszawa, Poland
[25] Rosseland Centre for Solar Physics, University of Oslo, PO Box 1029 Blindern, NO-0315 Oslo, Norway
[26] Space Sciences Lab, UC Berkeley, 7 Gauss Way, Berkeley, CA 94708, USA
[27] LESIA, UMR CNRS 8109, Observatoire de Paris, 5 place J. Janssen, 92195 Meudon, France
[28] Dublin Institute of Advanced Studies, 31 Fitzwilliam Place, Dublin 2, Ireland
[29] University of Central Lancashire, Preston PR1 2HE, UK

Citation: Lastname, F.; Lastname, F.; Lastname, F. The SPARK mission concept. *Aerospace* **2023**, *1*, 0. https://doi.org/

Received:
Revised:
Accepted:
Published:

30 Department of Physics, Astronomy and Mathematics, University of Hertfordshire, Hatfield AL10 9AB, UK
31 Centre Spatial de Liège, University of Liège (ULiège) – STAR Institute, Liège, Belgium
32 RAL Space, STFC Rutherford Appleton Laboratory, United Kingdom
33 Université Paris-Saclay, Université Paris Cité, CEA, CNRS, AIM, France
34 MIDA, Dipartimento di Matematica, Università di Genova, Genova, Italy
35 Department of Physics and Astronomy, University of Western Kentucky, Bowling Green, KY, USA
36 Osservatorio Astrofisico di Torino, Istituto Nazionale di Astrofisica, Pino Torinese, Italy
37 INAF – Osservatorio Astronomico di Roma, Monte Porzio Catone, Italy
* Correspondence: hamish.reid@ucl.ac.uk

Abstract: Particle acceleration is a fundamental process arising in many astrophysical objects including active galactic nuclei, black holes, neutron stars, gamma ray bursts, accretion disks, solar and stellar coronae, and planetary magnetospheres. Its ubiquity means energetic particles permeate the Universe and influence the conditions for the emergence and continuation of life. In our solar system, the Sun is the most energetic particle accelerator and its proximity makes it a unique laboratory in which to explore astrophysical particle acceleration. However, despite its importance, the physics underlying solar particle acceleration remains poorly understood. The SPARK mission addresses this need through a uniquely powerful and complete combination of γ-ray, X-ray, and EUV imaging and spectroscopy at high spectral, spatial, and temporal resolutions. SPARK's instruments will provide a step-change in observational capability, enabling fundamental breakthroughs in our understanding of solar particle acceleration and the evolution of solar explosive and eruptive events. In providing essential diagnostics for investigating the processes leading to flare and to coronal mass ejection onsets, SPARK will elucidate the underpinning science of space weather events which can damage satellites, disrupt telecommunications and GPS navigation, and endanger astronauts in space. The prediction of flares and CMEs, and mitigation against their potential impacts are crucial to protecting our terrestrial and space-based infrastructures.

Keywords: particle acceleration; magnetic reconnection; instrumentation; Sun: corona; Sun: coronal mass ejections (CMEs); Sun: flares; Sun: extreme ultraviolet Sun: X-rays, gamma rays

1. Scientific Objectives

The SPARK mission concept aims to investigate solar particle acceleration and the magnetic energy release that powers it by observing solar explosive and eruptive events, the most energetic and geo-effective drivers of space-weather.

In the standard model of solar eruptive events [Figure 1; see also 1], highly stressed magnetic fields reconnect in the low corona, thereby impulsively releasing vast amounts of energy. Depending on the magnetic configuration, plasma, magnetic field, and accelerated particles may escape into the heliosphere as coronal mass ejections (CMEs), "jets", or solar energetic particle events (SEPs) which directly contribute to space weather. Accelerated particles also spiral downward around magnetic field lines ("loops") towards the chromospheric "footpoints", depositing their energy as they propagate. This heats and ionises the plasma in the chromosphere, transition region (TR), and lower corona, producing the intense broadband radiation known as a solar flare. The rapid heating creates a high-pressure region that ablates material back up along the loops in a process known as chromospheric "evaporation" which causes the loops to radiate in extreme ultraviolet (EUV) and soft X-rays. Additionally plasma in and above the loops can be directly heated by the energy release and/or acceleration process.

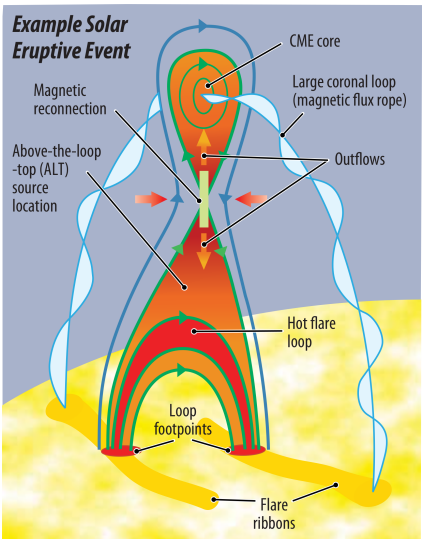

Figure 1. SPARK captures all elements of a solar eruptive event (the combination of a flare and a CME) identified in this cartoon. FOXSI images the HXR signatures of accelerated electrons and hot plasma at all locations. LISSAN captures the γ-ray signatures of accelerated ions and the most energetic electrons. And SISA reveals the lower at-

The particles in solar eruptive events can be divided into three populations: hot plasmas, accelerated electrons, and accelerated ions. One of most useful diagnostics for characterising thermalised and accelerated electrons is the X-ray bremsstrahlung emission they produce as they scatter in the ambient medium. The bremsstrahlung spectrum reflects the velocity distribution of the particles that produced it and can be inverted to reconstruct the spectrum of the emitting electrons [2,3]. This means hot plasma and accelerated electrons can be distinguished by their Maxwellian (thermal) and power-law (non-thermal) shaped spectra [e.g. 4–6]. Thermal emission tends to dominate in the soft X-ray (SXR; typically below 20 keV) regime while non-thermal emission tends to dominate in the hard X-ray (HXR; typically higher than 20 keV) regime. X-rays can provide straightforward measurements of the numbers and energies of accelerated electrons, not available from other wavelengths, or requiring non-trivial assumptions when observing in microwaves. X-rays can hence provide a deeper understanding of the underlying acceleration process.

Unlike energetic electrons, high-energy ions are even less understood due to the difficulties with their observational diagnostics. Accelerated ions in the range 1–100 MeV/nucleon can be detected via various γ-ray lines in the range 1–10 MeV due to nuclear de-excitation, neutron capture, and positron annihilation [7–14]. Higher energy ions can produce secondary pions via nuclear reactions with the ambient medium which then decay. The decay products produce a broad-band continuum at photon energies above 10 MeV with a broad peak around 70 MeV from neutral pion radiation. [15,16].

Although the principal points of the standard model are established, many questions remain regarding the fundamental processes of particle acceleration, impulsive energy release, and energy transport. However, the key science measurements to answer these questions have not been possible with previous instruments. Solar γ-ray line emission has been imaged in one flare [17], and localised through centroids in an additional four other flares [14]. Consequently the spatio-temporal evolution of accelerated ions has never been revealed. Hence the location and role of ion acceleration in solar eruptive events remains largely unknown, despite evidence that ions accelerated in flares may carry an energy comparable to that of accelerated electrons [e.g. 18–20]. Previous HXR spectroscopic imaging observations (e.g. RHESSI [21]; Solar Orbiter/STIX [22]) have not provided sufficient sensitivity to reliably observe accelerated electrons and direct plasma heating in the corona where the acceleration is believed to take place. This is because the intensity of bremsstrahlung depends on the ambient density which is typically very low in the corona, hence preventing observational tests of different acceleration models. Additionally, previous instruments have not provided sufficient dynamic range ($\geq$ 100) to simultaneously observe the emission from the corona and the chromosphere, where the density and hence emission, is much higher. This has limited our understanding of how transport effects alter the distribution of accelerated particles. Moreover, RHESSI was limited by its unfilled-aperture imaging technique that caused source areas and shapes to be only approximate, whilst imaging was unable to be taken on second and sub-second timescales, relevant to particle acceleration. Finally, current EUV imaging spectrographs (e.g. Hinode/EIS [23] and Solar Orbiter/SPICE [24]) have provided intriguing images of the complex structures associated with solar eruptive events but they have not been optimised for studying them. Their typical single slit design and operational priorities have led to EUV spectra rarely being available on the right timescales, at the right instances in time, and from the right locations to compare with X-ray and γ-ray observations.

SPARK will overcome all these challenges with its unique combination of high sensitivity fast spectroscopic imaging in γ-ray, X-ray, and EUV, optimised for solar eruptive events. It will address four specific fundamental science questions:

1. How does impulsive energy release accelerate particles in the solar atmosphere?
2. How is impulsively released energy transported and dissipated in the solar atmosphere?
3. What are the physical low-corona origins of space weather events?
4. How is the corona above active regions heated?

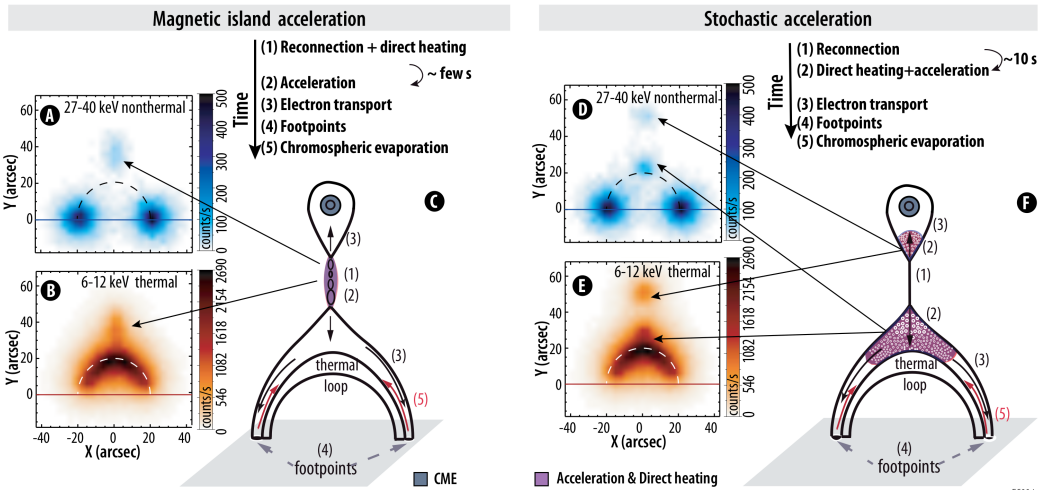

Figure 2. SPARK will distinguish between different models of flare particle acceleration. In these 2D flare cartoons, the locations and chronological order of various X-ray- and EUV-producing processes differ between the two most likely models of electron acceleration in eruptive flares: magnetic island-merging acceleration (left) and stochastic (second-order Fermi) acceleration (right). Simulated images of non-thermal electrons (blue) and thermal plasma (orange) are shown as insets. Figure courtesy of the FIERCE proposal team.

By addressing these questions, SPARK will elucidate fundamental physical processes that are ubiquitous throughout our Universe and drive space weather events that have direct consequences for our technologies and way of life.

1.1. How does impulsive energy release accelerate particles in the solar atmosphere?

Accelerated charged particles constitute a significant fraction (up to tens of percent) of the magnetic energy released in the most energetic space-weather events [e.g., 19,25]. Distinguishing between acceleration models observationally requires the number, location, and evolution of multiple faint thermal and non-thermal sources near the acceleration region in the corona to be characterized, in the presence of much more intense chromospheric footpoint emission. SPARK's unique combination of high dynamic range and high sensitivity imaging spectroscopy in the γ-ray, X-ray and EUV regimes, at timescales relevant to the underlying physical processes, will make this possible for the first time.

1.1.1. Where and when do particle acceleration and local plasma heating occur?

The two most likely models to explain the high acceleration efficiency of electrons are the Fermi acceleration process through evolving and merging "magnetic islands" [26,27] created by the reconnection, and a second-order Fermi acceleration process in the turbulent plasma of the reconnection outflow jets, with or without termination shocks [28–31]. The magnetic-island model predicts that both electron acceleration and direct plasma heating occur near the reconnection site(s) in the current sheet, and that direct plasma heating precedes the electron acceleration [26]. Conversely, the stochastic model predicts that acceleration and direct heating occur simultaneously, but significantly separated from the reconnection site in both upward and downward directed outflow jets. (See Figure 2.) Concerning ion acceleration, a detailed study of individual large events showed differences between ion and electron time evolution during the course of a flare [32]. The one flare imaged in the γ-ray line with RHESSI and the four flares that had centroid locations showed significant displacements between HXR and γ-ray line sources indicating spatial displacements between electron and ion energy release sites [14,17]. **SPARK will reveal, for the first time, where electron acceleration and direct heating occur with respect to the reconnection site, under what scenarios the different acceleration models are the dominant process, and reveal the relationship between electron and ion acceleration.** SPARK will compare γ-ray and X-ray signatures of energetic electrons and ions, in combination with the EUV non-Gaussian line profiles that are a signature of ion velocity distributions being non-Maxwellian. Using increased X-ray

sensitivity and dynamic range, SPARK will characterize the spectrum of the accelerated electrons in the corona, even in the presence of much brighter chromospheric emission. SPARK will provide complementary measurements of the coronal magnetic field from Fe X lines emitted around 1 MK, the plasma response to heating via the hot Fe XXIII and Fe XXIV (15–20 MK) spectral lines, and relative plasma abundances to differentiate between coronal plasma and ablated chromospheric plasma.

1.1.2. What is the efficiency and energy content of electron and ion acceleration?

The fraction of particles accelerated out of the ambient Maxwellian velocity distribution and the total energy they contain are essential constraints on acceleration models. Acceleration by magnetic islands [26] and super-Dreicer electric fields in a reconnecting current sheet [33] can accelerate a large fraction of the available electrons, while mechanisms relying on large-scale sub-Dreicer electric fields cannot [34]. **SPARK will determine the number and energy of accelerated particles with an accuracy not previously possible.** With improved X-ray dynamic range, SPARK will measure the non-thermal spectra of coronal and footpoint sources down to lower energies, whilst constraining the relative number of accelerated particles of different ion species [e.g. alpha/proton ratio; 32].

1.1.3. How electron and ion acceleration and transport differ in the flaring atmosphere?

Theoretical studies show that differences between the acceleration and transport of electrons and ions can be used as a unique diagnostic tool for the processes in the magnetic reconnection region, as well as the geometry of the magnetic field in and around it. Hence, the lack of observational information about ions, caused by the lack of spatially-resolved γ-ray observations, is a significant obstacle to constructing a comprehensive solar flare model. With LISSAN's spatial resolution of 8 arcsec, **SPARK will enable major advances in understanding how ions are accelerated and transported in flares and how their dynamics differ from the dynamics of energetic electrons**, and in using energetic ions as an important diagnostic tool for non-thermal plasma in the flaring corona.

1.1.4. Where and how are the most energetic particles accelerated at the Sun?

Studies of small numbers of events examining the γ-ray line (1–10 MeV) and pion continuum (>10 MeV) domains have suggested that the accelerated ion spectrum is not a simple power law extending from non-relativistic (1–100 MeV/nucleon) to relativistic (>few hundred MeV/nucleon) regimes [e.g. 35–39]. This raises the question of whether the most energetic particles are accelerated via a different mechanism to those at lower energies. The longevity of some pion emission presents another major challenge to our understanding of how the most energetic particles are accelerated at the Sun [e.g. 40,41]. **The high sensitivity HXR and γ-ray spectroscopy of SPARK will facilitate a comprehensive study of the timing and spectra of electron bremsstrahlung and pion decay radiation in a significant number of events for the first time.** Observations of the high-energy emissions are essential to unravel the relative roles of flare and interplanetary medium acceleration processes in accounting for high-energy ions, a question that is crucial to understanding long-duration events.

1.2. How is impulsively released energy transported and dissipated in the solar atmosphere?

SPARK will probe energy-transport processes that link impulsively released magnetic energy to the resultant emission from the lower atmosphere where the bulk of the flare energy is radiated. This will be done in two ways: by measuring hitherto poorly constrained observational inputs to the latest state-of-the-art numerical models of solar flares [e.g. 43–60], and; by providing previously unachievable observations against which the model predictions will be critically interrogated. Such model inputs provided by SPARK include the non-thermal electron and ion energy distributions injected towards the lower solar atmosphere, the ribbon/footpoint source areas, and the pre-flare atmospheric state (e.g. coronal temperature, density, loop length, and coronal magnetic field).

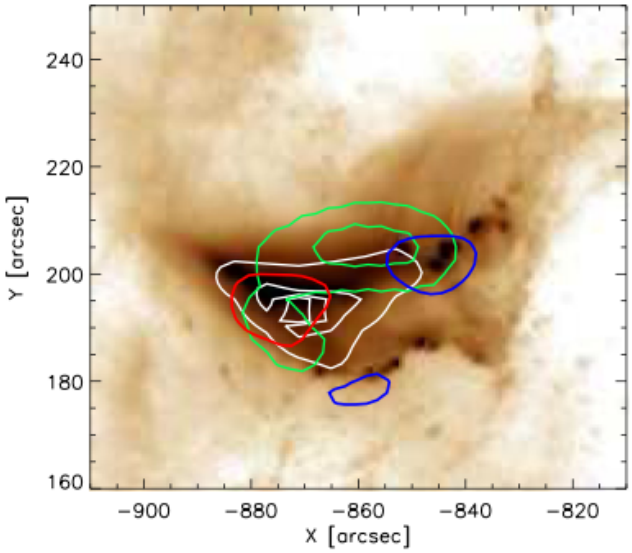

Figure 3. Combined X-ray and EUV spectroscopy analysis highlighting the presence of turbulence in a solar flare as a candidate mechanism for the transport of flare energy. Top: SDO/AIA 193 Å image (background); 50% RHESSI contours for 6 - 15 keV (red) and 25 - 50 keV (blue), EIS Fe XXIV (255 Å) at 30% and 75% contours (white), and Nobeyama 34 GHz radio emission at 30% and 75% contours (green). [42].

1.2.1. How and where do accelerated particles lose their energy in the corona and chromosphere?

As flare-accelerated particles exit the coronal acceleration region and propagate along loops, they lose energy through Coulomb collisions with ambient particles, wave-particle interactions, and the generation of return currents [4]. The evolution of the particle distribution as the particles propagate along flare loops depends on, and thus reveals, the relative importance of these mechanisms. The statistically significant separation between HXR and γ-ray line sources in the single resolved RHESSI γ-ray flare image and two of the four RHESSI centroid-localised γ-ray line flares [14,61] may be due to differing acceleration mechanisms. But it may also be due to different transport effects acting on the ions and electrons. We have sparse observations from EUV imaging spectrometers of the kernels of chromospheric evaporation, showing large non-thermal broadenings and upflows in the hotter lines during the impulsive phase [see e.g. 62–64], but a clear picture is missing. **SPARK will simultaneously observe electrons throughout the flaring structure, image ion emission, and observe the spectral line response of flaring plasma at multiple temperatures**. Combining X-rays and EUV imaging spectroscopy, SPARK will facilitate accurate determination of the low-energy part of the electron spectrum, as well as quantifying return current losses. SPARK will for the first time constrain accelerated ions transported to the chromosphere using γ-rays and the hottest EUV flare lines like Fe XXIV. Moreover, the combination of X-rays and the multi-temperature response of spectral lines will also provide constraints on turbulence present in the solar atmosphere [42], illustrated in Figure 3 .

1.2.2. What are the origins of modulations in solar flare emission?

A key observational feature in flare-associated X-ray emission is the presence of pronounced pulsations and fast-time variations. These modulations, which also appear in many stellar flares, are identified in both the non-thermal and thermal X-ray observations across all wavelength regimes from radio to gamma-rays, with characteristic timescales ranging from 0.5 to tens of seconds [e.g., 65–67]. Often, these modulations appear as regular or non-stationary oscillatory patterns, known as “quasi-periodic pulsations” [e.g., 68,69]. However, despite years of research in the temporal domain, we still do not know whether they are a direct signature of a repetitive impulsive energy release process or related to magnetohydrodynamic (MHD) oscillations in the flaring site or nearby, or some combination of those processes. Moreover, it is quite likely that different classes of flaring pulsations are produced by different mechanisms. X-ray dynamic range limitations have not yet allowed us to identify time-varying signatures from different parts of the loop, including the loop-top

source. EUV imaging observations have also hindered our ability to locate the modulating emission source due to both cadence constraints and pixel saturation and bleeding during flare events. **SPARK enables, for the first time, a full examination of the temporal, spatial and spectral properties of these pulsations and their relationships across wavelengths, which is essential to determine the origins of the emission modulation.** SPARK will allow us to identify the pulsations in both the thermal and non-thermal regimes in all parts of the flaring loop. Moreover, SPARK will identify whether accelerated protons have similarly associated time-variability.

1.2.3. What is the importance of accelerated particles in transporting energy with that of other mechanisms?

High frequency Alfvén waves have been proposed as a means of transporting energy from a flare's magnetic reconnection site to the lower atmosphere and heating it [e.g. 70–72]. In recent years, modelling has shown that this is possible [49,57,58]. However, while Alfvén waves are undoubtedly produced during the large scale reconfiguration of the magnetic field during flares, it is not yet known whether they play a significant role relative to accelerated particles in transporting flare energy and heating flare plasma, and whether other kinds of MHD waves, such as kink and sausage modes could contribute to the process. **SPARK will, for the first time, reveal the importance of MHD waves relative to accelerated particles in transporting and dissipating energy in solar eruptive events, from the energy release site throughout the lower solar atmosphere.** SPARK will examine the coronal magnetic field strength and the broadening of certain spectral lines from ions in the EUV passbands formed at different temperatures, constraining the Poynting flux as the waves propagate and dissipate their energy [see discussion in, e.g., 73]. SPARK will use variations of the chemical composition and elemental abundances to assess the role of MHD waves in transferring energy from the corona into flare kernels [cf. 74, and references therein].

1.3. What are the physical low-corona origins of space weather events?

An ESA-funded study has estimated that the economic cost of a severe space weather event could be as high as €15 billion[1]. This led to the establishment of national forecasting centres across Europe and space weather as a major theme in ESA's Space Safety programme. Despite this, many questions remain regarding the origins of space weather in the low-corona which act as an impediment to the development of timely and reliable space weather forecasts. **SPARK will greatly improve our understanding of the underlying physical processes that drive these events in the low corona and inform development of future space weather models that aim to deliver timely and accurate forecasts of flaring, energetic particles and eruptive events.** Knowing about the acceleration process will feed into understanding how active regions reach a state whereby a flare or CME is generated. Understanding of the flare initiation process will enable an improved view of the likelihood of a flare occurring in a location that is well placed to impact Earth.

1.3.1. What is the energy content and spectrum of Sun-escaping electrons?

Sun-escaping electrons, a component of SEP space weather events, have long been studied in situ at 1 AU [75] and more recently closer to the Sun [e.g. 76,77]. However such observations alone cannot be used to characterise how the electrons are accelerated because the electron distribution is modified by transport effects between the Sun and the observatory. SEP electrons can be observed remotely at the Sun as type III radio bursts [e.g. 78,79, as reviews]. However while bulk electron speeds can be inferred from the radio observations, they, unlike X-rays, cannot be directly inverted to retrieve the numbers or energies of accelerated electrons. Therefore, the spectra and acceleration mechanism(s) of solar radio emitting electrons remains unknown. How these accelerated electrons escape from the flare site is similarly unknown. CMEs and jets offer clear open magnetic paths for particles to escape, but confined flares do not although interchange reconnection can pay a role [80]. Ground-based observations above 10 MHz can be used to image type IIIs [81] but may suffer especially at low frequencies from intrinsically limited spatial resolution on account of the radio waves scattering off density inhomogeneities between the source and observer [82,83]. **SPARK will**

[1] https://esamultimedia.esa.int/docs/business_with_esa/Space_Weather_Cost_Benefit_Analysis_ESA_2016.pdf

provide hitherto unachievable imaging and spectral observations of the accelerated electrons as they escape the Sun [84], facilitated by unprecedented sensitivity and imaging dynamic range in the HXR regime. Such measurements will elucidate the origins of escaping electrons and how they are modified as they propagate towards Earth. SPARK will also test theories of the origins of the slow solar wind by detecting the locations at active region peripheries where particles are accelerated and escape via HXR emissions and upward flows detected in EUV emitting plasma.

1.3.2. What are the dominant initiation mechanisms of solar eruptions?

Many models for the initiation of solar eruptive events involve magnetic reconnection, which results in plasma heating [85,86] and particle acceleration [87]. However, different models of CME initiation predict observationally differentiable locations of the erupting flux rope in relation to where the reconnection starts, and consequently for the associated X-ray and EUV emissions. The internal tether cutting model [88,89] predicts that reconnection occurs below the flux rope before the fast take-off of the eruption, the breakout model [90] predicts that the reconnection occurs above the flux rope before fast take-off, and the ideal MHD instability model [91] predicts that the flux rope begins to rise before reconnection occurs in either place. It is unclear if the same mechanisms driving the large-scale CMEs are also at play in these smaller events. Some models for jets involve breakout reconnection [e.g. 92] similar to the breakout model for CMEs, while others involve interchange magnetic reconnection [93–95]. **SPARK will produce observations of the faint X-ray and EUV emission linked to particle acceleration and plasma heating during the formation and initiation of solar eruptions for the first time.** This will provide an ability to discriminate between the many physical processes proposed to be responsible for bringing the corona to a state in which an eruption is possible. SPARK will also provide measurements of the plasma dynamics and of the magnetic field of the active region and filament before and during the eruption, providing constraints on the configuration and evolution of the magnetic structure leading to solar eruptions.

1.4. How is the corona above active regions heated?

A long-standing enigma in solar and stellar physics is how a star's atmosphere can be orders of magnitude hotter than its surface. This temperature difference requires some form of non-radiative heating, but whether the dominant mechanism is the dissipation of Alfvén waves or impulsive heating by nanoflares has not been established [96–100]. SPARK will enable breakthroughs in this fundamental problem using two approaches. First, SPARK will determine if the characteristics of energy release in the smallest detectable events are fundamentally different from those in larger flares. Second, SPARK will statistically determine ensemble properties of heating events too small to be detected individually.

1.4.1. Is particle acceleration ubiquitous among energy release events at all size scales?

The number of flares as a function of their thermal energy follows a power-law over several orders of magnitudes [101]. This suggests that the underlying energy-release process scales similarly. If nanoflares are part of this distribution, they too would be expected to accelerate electrons. Indirect evidence from UV transients suggests that accelerated electrons are indeed present [102,103]. RHESSI and STIX observations have shown that, in microflares, the X-ray spectral index is steeper than in larger flares [104–110], suggesting that they are less efficient at accelerating electrons. This was confirmed in a few observations of fainter microflares with NuSTAR, during its limited solar campaigns [111–113]. Additional support comes from studies of the thermal-nonthermal energy partition [cf. 114], which show that in weaker flares there may not be sufficient energetic electrons to heat the thermal plasma. **SPARK will determine how the energy release process scales across 8 orders of magnitude in energy from the largest flares (~10^{33} ergs) down to flares at 10^{25} ergs** (2 orders of magnitude smaller than those observed by RHESSI and STIX). SPARK will observe hundreds of thousands of flares below GOES C class and will provide a comprehensive investigation of events two orders of magnitude less energetic than ever before.

1.4.2. How does small-scale particle acceleration contribute to coronal heating?

The presence of temperatures exceeding 5 MK in the non-flaring active regions would provide strong evidence of impulsive, low-frequency nanoflare heating. Steady or high-frequency wave heating cannot maintain such high temperatures without violating other observational constraints [99,115]. Many studies have detected hot plasma [e.g. 116,117], but the uncertainties are large because the emission is orders-of-magnitude fainter than that from associated cooler plasma [cf. the review in 118]. Moreover, non-equilibrium ionization effects [119–121] and departures from a Maxwellian distribution due to the presence of accelerated particles [103,122–124] can limit the interpretation of EUV line emission observations. SXR and HXR thermal bremsstrahlung emission from the same plasma are not susceptible to non-equilibrium ionization effects, allowing measurements to be more clearly interpreted, and the accelerated particles to be more readily detected. The FOXSI-2 sounding rocket made X-ray measurements of high-temperature plasma in an active region [125] and SXR spectrometers flown on the SDO/EVE sounding rocket [117] and on the MinXSS CubeSat [126] have made high-temperature measurements from spatially integrated SXR spectra. These measurements provide evidence of impulsive magnetic-reconnection events contributing to active-region heating [127]. **SPARK will provide important constraints on competing scenarios of coronal heating in active regions** [128,129]. SPARK will directly measure the predicted high-temperature X-ray signature of low-frequency nanoflare heating, improved by observations of multiple coronal emission lines from many ionisation states of Fe. Some of these lines also allow diagnostics of accelerated electrons [122,124]. Ionization and recombination timescales will be derived through observations of the density of hot plasma, a key measurement not provided by prior EUV observations/missions. Furthermore, SPARK will also provide measurements of magnetic field strengths in active region loops, using the magnetically induced transition at 257.3 Å [cf 130, and references therein].

2. Payload

The SPARK satellite is a solar-dedicated observatory to study particle acceleration in multiple forms of solar activity, by performing imaging spectroscopy in the γ-ray, X-ray and EUV regimes. SPARK utilises three scientific instruments to provide detailed imaging spectroscopy across this large range in wavelength: LISSAN, FOXSI and SISA. Figure 4 shows a model of the spacecraft, highlighting the accommodation of the three scientific instruments.

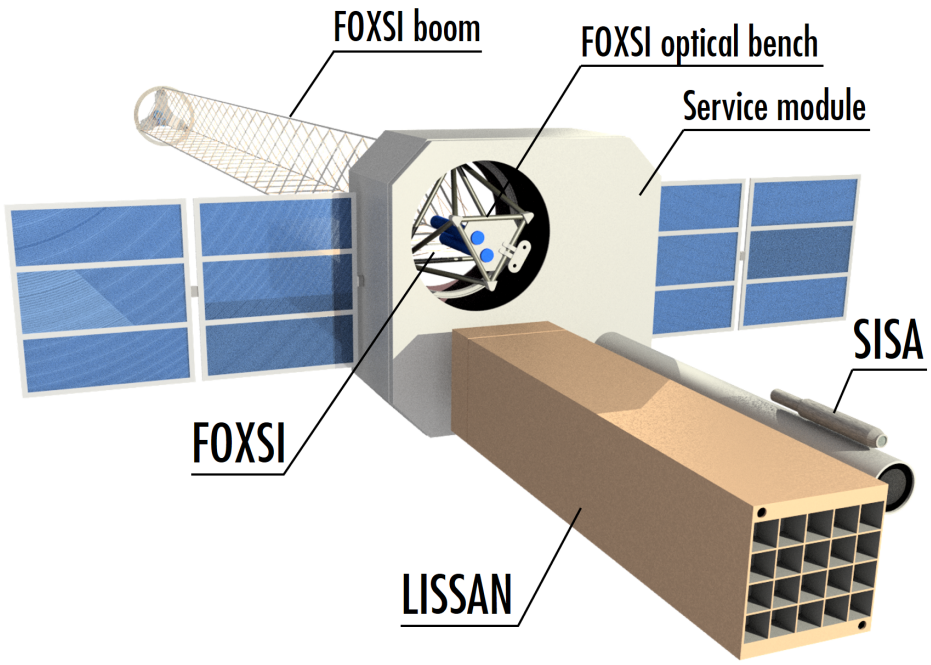

Figure 4. SPARK spacecraft model illustrating the payload accommodations.

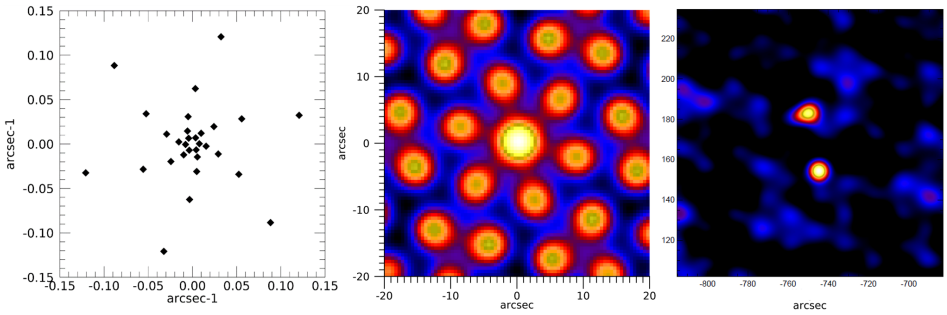

Figure 5. Left: One possible (u, v)-coverage for LISSAN; Middle: associated point spread function (dirty map of a point source on-axis: this image contains both the X-ray source and instrumental artefacts to be removed with adequate cleaning algorithms); Right: Simulation of a LISSAN image of the 50-84 keV emission from the two hard X-ray footpoints during the M9.7 flare on 31st March 2022, which was observed by STIX on Solar Orbiter. This image was obtained by running the CLEAN algorithm on the dirty image.

2.1. Large Imaging Spectrometer for Solar Accelerated Nuclei (LISSAN)

LISSAN will, for the first time, reveal the dynamics of accelerated ions in solar flares via spectroscopic imaging between 40 keV and 100 MeV on timescales of less than 10 s (add reference to LISSAN paper here). LISSAN will also observe high energy X-ray emission from energetic electrons, thus providing diagnostics of both types of accelerated particles. This will be achieved by using high-resolution scintillators with an energy resolution of 0.1 MeV at 6.1 MeV and angular resolution of 8" FWHM. LISSAN employs an indirect Fourier imaging technique [131,132] with pairs of grids or bigrids above the detectors encoding information on the angular distribution of the flaring X-ray source into Moiré patterns on the detectors, each of which corresponds to a given Fourier component (or *visibility*). This imaging concept, using spatially sensitive detectors, was pioneered on the STIX [22,133] instrument onboard Solar Orbiter.

The LISSAN instrument is composed of 20 sub-collimators. 15 contain bigrids for imaging spectroscopy. Of the remaining 5 without bigrids, one will monitor the background and 4 are used for spectroscopy only. The absence of bigrids leads to a factor 4 improvement in sensitivity. Each sub-collimator contains a detector formed up of sixteen "fingers" of crystal. In one direction, this segmentation allows the moiré pattern to be resolved, whilst the other direction improves light collection and therefore spectral resolution, and provide a redundant measurement of the moiré pattern. This guarantees the energy resolution (better than 1.5% FWHM at 6.1 MeV) needed to measure the Doppler profiles of the C and O lines at 4.4 and 6.1 MeV. LISSAN will achieve 40x RHESSI's sensitivity (5 counts/cm^2) and 1.5 %dE/E at 6.1 MeV and a range of 40 keV–100 MeV and 40x RHESSI's sensitivity (50 counts/cm^2) in the 2.2 MeV neutron capture line. A summary of the predicted performance of LISSAN is presented in Table 1.

LISSAN Parameter	Expected Performance
Energy Range - Low	40 keV
Energy Range - High	100 MeV
Imaging Effective Area (2.2 MeV)	100 cm^2
Spectro Effective Area (2.2 MeV)	440 cm^2
Sensitivity (2.2 MeV)	50 counts/cm^2
Sensitivity (6.1 MeV)	5 counts/cm^2
Imaging Time Resolution	1 s
Angular Resolution	8"
Field of View	12.8' diameter
Energy Resolution (6.1 MeV)	1.5% dE/E
Largest Observable Flare	>X5

Table 1. LISSAN instrument performance

The LISSAN imaging system contains 15 sub collimators, which consist of a detector array and a pair of grids in front of it. Therefore, the instrument measures 15 visibilities. The angular frequencies sampled by the instrument in the Fourier space, or (u, v)-plane, are determined by hardware parameters of the sub collimators (e.g. grid orientation and pitch). One possible distribution of the set of frequencies measured by LISSAN (or (u, v)-coverage) and the associated point spread function, are displayed in Figure 5.

2.2. Focusing Optics X-ray Solar Imager (FOXSI)

Table 2. Expected Performance of SPARK/FOXSI.

FOXSI Parameter	Expected Performance
Energy Range - Low	3 keV
Energy Range - High	55 keV
Imaging Dynamic Range 1	20:1 beyond 20” separation
Imaging Dynamic Range 2	1000:1 beyond 45” separation
Effective Area (at 20 keV)	40 cm^2
Sensitivity	0.2 photon / cm^2
Imaging Time Resolution	0.1 s
Angular Resolution	6.3” FWHM
Field of View	9.8’×9.8’
Energy Resolution	0.7 keV FWHM
Largest Observable Flare	>X10

FOXSI combines grazing incidence hard X-ray focusing optics with small, fast, pixelated detectors to produce images of the Sun at high spectral, spatial and temporal resolution over the spectral range 3–50 keV. This strategy offers dramatic improvements in image quality, dynamic range and sensitivity over the indirect (Fourier-based) imaging techniques of current and previous state-of-the-art solar X-ray spectroscopic imagers, e.g. RHESSI and Solar Orbiter/STIX. This will allow FOXSI to reliably image faint thermal and non-thermal sources in the solar corona, even in the presence of brighter ones, for the first time. This makes FOXSI ideal to enable a ground-breaking new understanding of particle acceleration and the evolution of solar eruptive events. FOXSI does not intrinsically integrate images over preset time or energy intervals but instead records the energy, position and arrival time of individual photons. This enables scientists to produce images and spectra ex-post-facto in accordance with their science goals. FOXSI’s design and measurement strategy has been proven through successful flights of several solar sounding rocket and balloon instruments [134–139]. Moreover, FOXSI will build on the success of non-solar space-based direct focusing X-ray imagers (e.g. NuSTAR, Hitomi) while being optimised for the high fluxes and resolution requirements of solar observations. A summary of the predicted performance of FOXSI is presented in Table 2.

Table 3. Expected Performance of SPARK/FOXSI-STC.

FOXSI-STC Parameter	Expected Performance
Energy Range - Low	0.8 keV
Energy Range - High	15 keV
Effective Area	0.01 cm^2
Energy Resolution	0.2 keV FWHM below 1.5 keV
Field of View	9.8’×9.8’
Time Resolution	0.5 s
Largest Observable Flare	>X10

FOXSI also includes a soft X-ray spectrometer (FOXSI-STC) that provides high spectral resolution, spatially-integrated spectra in the spectral range 0.8–15 keV. The combination of emission lines and thermal continuum emission in this energy range provides additional plasma temperature

and composition information averaged over all the plasma in the FOXSI FOV that FOXSI does not have access to due to its lower energy resolution and higher low energy cutoff. FOXSI-STC is composed of two identical spectrometers with different apertures optimised for low and high flux, respectively.

FOXSI-STC can measure the X-ray fluxes for even the largest flares and will be used to control removable FOXSI attenuators. This approach will enable fewer attenuator motions compared to past and current instruments which have to frequently remove their attenuators for short periods of time (i.e. peek) to check whether the flux has reduced to an acceptable level. A summary of the predicted performance of FOXSI-STC is presented in Table 3.

2.3. Spectral Imager of the Solar Atmosphere (SISA)

Table 4. Instrument requirements and expected performance of SISA.

SISA Parameter	Expected Performance
Spectral Window 1	178–184 Å
Spectral Window 2	221–264 Å
Spectral Resolution	0.05 Å FWHM
Spectral Resolving Power (R)	3560–5160
Field of View	100”×250”
Spatial Resolution	1” in 2 pixels
Temporal Resolution (high signal)	1 s
Temporal Resolution (low signal)	10 s

SISA (Spectral Imaging of the Solar Atmosphere) is an integral field spectrograph (IFS), providing the simultaneous spectra of a bi-dimensional field of view of 100 arcseconds by 250 arcseconds using image slicer technology (add reference to SISA paper here). Two spectral ranges will be covered, centred around 18.5 nm and 25 nm, with 1 arcsecond spatial resolution and a spectral resolving power R ~ 3650–5160. A spectral range of 170-195 Å and 245-260 Å is required to measure the parameters of both 1 MK plasma and the hotter 15 MK plasma. This wavelength range includes lines sensitive to coronal magnetic field [Fe X 25.7 nm, see e.g. 130,140,141] and electron temperature / non-Maxwellian electron distributions [142,143]. It also has a wide range of lines to measure electron densities from coronal (e.g. Fe IX, Fe XI, Fe XII, Fe XV, Ca XV) to flare temperatures (Fe XXI), and the FIP bias. It observes He II and a wide range of lines, many at flare temperatures (e.g. Fe XVII, Fe XX, Fe XXI, Fe XXII, Fe XXIII, Fe XXIV).

In order to achieve the temporal resolution of 1 second, required to capture the rapid development of the plasma environment during flare energy release, the observation of a 2-D field of view simultaneously, without the traditional use of slit scanning systems, is a key factor. The Integral Field Spectroscopy technique is a novel proposal for the Extreme Ultraviolet (EUV) regime and benefits from a wide heritage of integral field spectrographs operating at ground-based and space-based telescopes. This strategy has significant advantages over traditional EUV scanning spectroscopy (e.g. EIS, IRIS, Solar-C/EUVST), making 2D images over two orders of magnitude faster than before. Compared to the upcoming Multi-Slit Solar Explorer [MUSE; 144] spacecraft, SISA will capture the full field of view 10 times faster. The wavelength range of SISA is both different and wider than that of MUSE, offering a wide array of plasma diagnostics so that 2D maps of, for example, electron density (at multiple temperatures) and magnetic field will be obtained. We note that several SISA diagnostics such as the measurements of coronal magnetic fields and departures from electron Maxwellian distributions are not available to SOLAR-C/EUVST. A summary of the predicted performance of SISA is presented in Table 4. The ability to obtain diagnostics at 1 s cadence is based on estimates of the signal in active region cores and flares and the strawman design (described in the SISA paper), consisting of a single multi-layer for the three reflecting surfaces and a 20 cm aperture of the off-axis telescope.

SISA will be composed of two subsystems: the telescope, an off-axis parabolic mirror and the integral field spectrograph, an array of curved slicer mirrors and curved gratings. The slicer mirrors are placed at the telescope focus and decompose (slice) the image of the field of view using an array

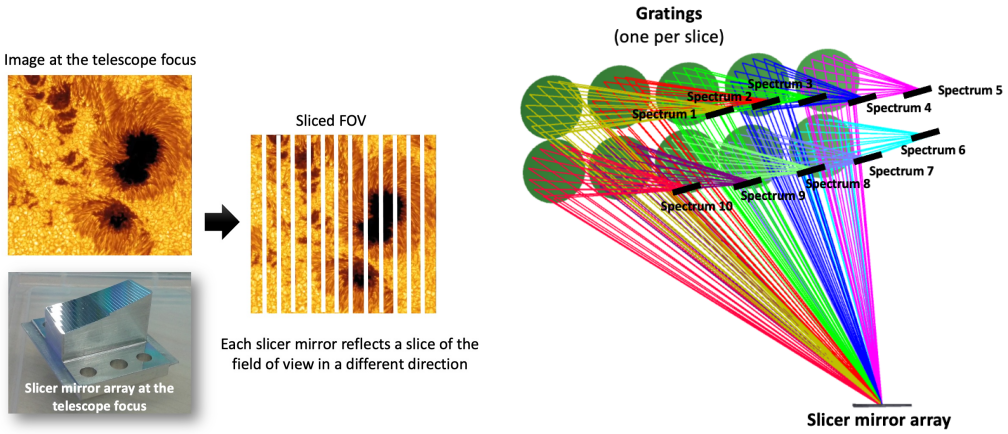

Figure 6. Left: Sketch of an image slicer functionality. The image slicer acts as a field reformatter, slicing the entrance field of view and generating a pupil per slice. (Note that despite apparent gaps in the sliced FOV in the figure, the sliced FOV provides a contiguous map when combined.) Right: SISA conceptual layout with a reduced number of slicers. Each curved grating produces the spectrum of each slice of the field. The tilt angles of the gratings offer flexibility in the geometrical distribution of the spectra on the detector.

Table 5. Required resources for LISSAN, FOXSI, including FOXSI-STC, and SISA.

Resource	LISSAN	FOXSI	SISA
Mass	370 kg	120 kg	78 kg
Volume	1.96 m^3	$(105\ cm)^3$ (stowed)	0.5 m^3
Power	125 W (peak)	170 W (average)	130 W (average)
Data Rate	25 Mbits/s (peak)	1 Mbits/s (peak)	50 Mbits/s (average)
Operating Temp	0°C (FEE)	-20–0°C (FPA)	< −40 °C (FPA)

of powered mirrors with rectangular shape, each one of them with a different tilt angle around the X and Y axes. These will produce a pupil image per slice reflected in different directions towards the curved gratings, which perform three functions: (i) dispersion of the incoming beam into its constituent wavelengths; (ii) imaging the beams on the detector with the required magnification and (iii) controlling the location of the exit pupil. The orientation of the gratings are fixed. Each grating will produce the spectrum of each slice of the field, as shown in Figure 6. The tilt of each grating will be defined to distribute the spectra on the detectors. SISA will be the first integral field spectrograph in the EUV spectral range.

2.4. Mass and Power

The required resources for LISSAN, FOXSI including FOXSI-STC, and SISA are given in Table 5. The mass estimates include a 20% margin on each instrument whilst the power requirements include a 30% margin on each instrument. The operating temperatures are the most stringent constrains for each instrument, relevant for the Frond End Electronics (FEE) for LISSAN, and the Focal Plane Assembly (FPA) for both FOXSI and SISA.

3. Proposed Mission Configuration and Profile

To meet its science objectives, SPARK must be launched at a time when medium to large solar flares can be observed. This can be achieved at any time in the solar cycle except solar minimum.

3.1. System level requirements

A pointing accuracy of 10 arcsecs is required due to the FOV of all SPARK's instruments, and the need to point to a chosen active region. The Performance Drift Error (PDE) is driven by the spatial resolution of SISA and is 0.1 arcsec within a time interval of one second. The requirement will be fulfilled by further attenuating the spacecraft PDE with a tip-tilt system. Each instrument

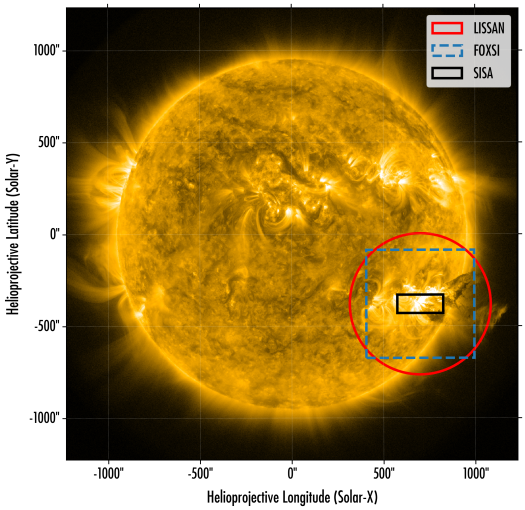

Figure 7. Fields of view of the three imaging instruments of SPARK overplotted on the EUV 171 Sun from AIA.

suite will carry its own aspect system to overcome uncertainty in the co-alignment between the instruments, as the precise knowledge of the position of the γ-ray, X-ray and EUV emissions relative to one another is key to fulfil the scientific objectives of the mission. Therefore, each instrument will provide precise knowledge of the pointing.

LISSAN and the FOXSI HXR telescopes will be operating in one nominal observing mode. SISA will have two operational modes. The first mode (cadence 1) will be for observing flaring active region, when there is an abundance of EUV radiation. The second mode (cadence 2) is when the Sun is less active and the signal is weaker, requiring slower exposure times. A safe mode will be implemented for each instrument to react to instrument or spacecraft failure.

3.2. Operations

The SPARK payload is designed to provide synchronized observations that address specific science questions. Since the instruments will always observe the same targets, the science operations will not require a large degree of flexibility. As instruments have a FOV smaller than the Full Sun, target selection will be required. Targets will typically be solar active regions most likely to produce energetic flares. SPARK will allow the community to submit observing plans for targeted observations.

Science and housekeeping data recorded in the onboard mass memory will be brought down in raw format, for processing on the ground into level 0 format. The nature of multiple downlink stations may require that data are aggregated and sorted before this processing. Further pipeline processing will bring data to level-2 derived products, via level-1 calibrated data. Minimal data processing will happen on board, and all the data will be downlinked for processing on ground.

3.3. Spacecraft design

Primary drivers for the SPARK spacecraft design are the accommodation of the extendable boom for FOXSI and the large mass of LISSAN. The boom will be deployed in orbit and alignment between the optics on the spacecraft and the detectors at the tip of the extendable structure will be performed using the FOXSI tip/tilt mechanism.

SPARK's payload includes imaging instruments and thus requires a 3-axis system to minimise spatial blurring. The combination of individual instrument stability requirements leads to an overall requirement for the PDE of 0.1" over 1 second. The spacecraft Absolute Performance Error or APE is 10" to allow a 10% error on the smaller SISA field of view pointing at the correct target. The requirement for the Relative Performance Error (RPE) is 1" for integration times of 1 s. The attitude sensors should include a fine Sun sensor and a star tracker in order to determine spacecraft pointing relative to the Sun. An inertial reference unit is required to determine changes of attitude with time.

SPARK's baseline L1 orbit provides a stable thermal environment such that the thermal control on the instruments can maintain any required temperature. The spacecraft will have one side constantly facing the Sun and one side facing cold space all the time. SPARK's thermal requirements can be met by a passive cooling system consisting of cold fingers and radiators.

SPARK will provide science data downlink to Earth using a K-band 26 GHz antenna. Even with a reduced ground station contact of 4 hours to obtain 850 Gbits/day (similar to Euclid), this would be enough to downlink the entire maximum daily data volumes of 80 Gbit (LISSAN) and 86 Gbit (FOXSI). The SISA maximum daily data volume of 4.3 Tbits/day would be stored using on-board Mass Memory storage of at least 4 TB, with synoptic data being communicated to the Earth to choose a subset of events to download and/or periods to downlink with reduced cadence.

4. Current status of SPARK

The initial SPARK proposal was initially submitted to ESA in 2010 as an M-class mission that included a modified version of LISSAN and FOXSI, with different supporting instruments. More recently the relevant particle acceleration and transport topical questions were presented as an ESA Voyage 2050 white paper in 2020, and subsequently published [145].

The SPARK proposal in this current form was proposed to ESA in 2022 as an M-class mission, and reached Phase-2. Development of the individual instruments proposed for SPARK continues, funded by ....

There is clear support for the goals and implementation of SPARK across the broad European scientific community in solar physics and beyond. We foresee the implementation of SPARK in this form presents an exciting opportunity for paradigm-shifting observations in the field of astrophysical particle acceleration and transport, using data from our local laboratory, the Sun.

Author Contributions: For research articles with several authors, a short paragraph specifying their individual contributions must be provided. The following statements should be used "Conceptualization, X.X. and Y.Y.; methodology, X.X.; software, X.X.; validation, X.X., Y.Y. and Z.Z.; formal analysis, X.X.; investigation, X.X.; resources, X.X.; data curation, X.X.; writing—original draft preparation, X.X.; writing—review and editing, X.X.; visualization, X.X.; supervision, X.X.; project administration, X.X.; funding acquisition, Y.Y. All authors have read and agreed to the published version of the manuscript.", please turn to the CRediT taxonomy for the term explanation. Authorship must be limited to those who have contributed substantially to the work reported.

Funding: Please add: "This research received no external funding" or "This research was funded by NAME OF FUNDER grant number XXX." and and "The APC was funded by XXX". Check carefully that the details given are accurate and use the standard spelling of funding agency names at https://search.crossref.org/funding, any errors may affect your future funding. JD was funded by the Czech National Science Foundation, Grant No. GACR 22-07155S. JD and JK were supported by the project RWO:67985815. DML is grateful to the Science Technology and Facilities Council for the award of an Ernest Rutherford Fellowship (ST/R003246/1).DOS acknowledges financial support from the grants AEI/MCIN/10.13039/501100011033/(RTI2018-096886-C5, PID2021-125325OB-C5, PCI2022-135009-2) and ERDF "A way of making Europe" and "Center of Excellence Severo Ochoa" award to IAA-CSIC (CEX2021-001131-S). SM and TM were supported by the National Science Centre, Poland grant No. 2020/39/B/ST9/01591.

Data Availability Statement: No new data were created or analyzed in this study. Data sharing is not applicable to this article.

Acknowledgments: In this section you can acknowledge any support given which is not covered by the author contribution or funding sections. This may include administrative and technical support, or donations in kind (e.g., materials used for experiments).

Conflicts of Interest: The authors declare no conflict of interest.

Abbreviations

The following abbreviations are used in this manuscript:

AIA	Atmospheric Imaging Assembly
CME	Coronal Mass Ejection
EIS	EUV Imaging Spectrometer onboard Hinode
EUV	Extreme Ultraviolet
EUVST	Extreme Ultraviolet High-Throughput Spectroscopic Telescope
EVE	EUV Variability Experiment onboard SDO
FEE	Front-end Electronics
FIERCE	Fundamentals of Impulsive Energy Release in the Corona Explorer
FPA	Focal Plane Assembly
FOV	Field Of View
FOXSI	Focusing Optics X-ray Solar Imager
FOXSI-STC	FOXSI's Spectrometer for Temperature and Composition
FWHM	Full Width Half Maximum
GOES	Geostationary Operational Environmental Satellite
HXR	Hard X-ray
IFS	Integral Field Spectrograph
IRIS	Interface Region Imaging Spectrograph
LISSAN	Large Imaging Spectrometer for Solar Accelerated Nuclei
MHD	Magnetohydrodynamic
MUSE	Multi-Slit Solar Explorer
NuSTAR	Nuclear Spectroscopic Telescope Array
RHESSI	Reuven Ramaty High Energy Solar Spectroscopic Imager
SDO	Solar Dynamics Observatory
SEP	Solar Energetic Particle
SISA	Spectral Imager of the Solar Atmosphere
SPARK	Solar Particle Acceleration, Radiation and Kinetics mission
STIX	Spectrometer/Telescope for Imaging X-rays
SXR	Soft X-ray

References

1. Shibata, K. New observational facts about solar flares from YOHKOH studies - evidence of magnetic reconnection and a unified model of flares. *Advances in Space Research* **1996**, *17*, 9–18. https://doi.org/10.1016/0273-1177(95)00534-L.
2. Brown, J.C. The Deduction of Energy Spectra of Non-Thermal Electrons in Flares from the Observed Dynamic Spectra of Hard X-Ray Bursts. Sol. Phys. **1971**, *18*, 489–502. https://doi.org/10.1007/BF00149070.
3. Piana, M.; Massone, A.M.; Kontar, E.P.; Emslie, A.G.; Brown, J.C.; Schwartz, R.A. Regularized Electron Flux Spectra in the 2002 July 23 Solar Flare. ApJ **2003**, *595*, L127–L130. https://doi.org/10.1086/378171.
4. Holman, G.D.; Aschwanden, M.J.; Aurass, H.; Battaglia, M.; Grigis, P.C.; Kontar, E.P.; Liu, W.; Saint-Hilaire, P.; Zharkova, V.V. Implications of X-ray Observations for Electron Acceleration and Propagation in Solar Flares. Space Sci. Rev. **2011**, *159*, 107–166, [arXiv:astro-ph.SR/1109.6496]. https://doi.org/10.1007/s11214-010-9680-9.
5. Kontar, E.P.; Brown, J.C.; Emslie, A.G.; Hajdas, W.; Holman, G.D.; Hurford, G.J.; Kašparová, J.; Mallik, P.C.V.; Massone, A.M.; McConnell, M.L.; et al. Deducing Electron Properties from Hard X-ray Observations. Space Sci. Rev. **2011**, *159*, 301–355, [arXiv:astro-ph.SR/1110.1755]. https://doi.org/10.1007/s11214-011-9804-x.
6. Benz, A.O. Flare Observations. *Living Reviews in Solar Physics* **2017**, *14*, 2. https://doi.org/10.1007/s41116-016-0004-3.
7. Chupp, E.L. High-Energy Neutral Radiations from the Sun. ARA&A **1984**, *22*, 359–387. https://doi.org/10.1146/annurev.aa.22.090184.002043.
8. Ramaty, R. Nuclear processes in solar flares. In Proceedings of the Physics of the Sun. Volume 2, 1986, Vol. 2, pp. 291–323.
9. Chupp, E.L. Evolution of our understanding of solar flare particle acceleration: (1942-1995). In Proceedings of the High energy solar Physics; Ramaty, R.; Mandzhavidze, N.; Hua, X.M., Eds., 1996, Vol. 374, *American Institute of Physics Conference Series*, pp. 3–34. https://doi.org/10.1063/1.50997.
10. Trottet, G.; Vilmer, N. The Production of Flare-Accelerated Particles at the Sun. In *European Meeting on Solar Physics*; Simnett, G.M.; Alissandrakis, C.E.; Vlahos, L., Eds.; Springer-Verlag, 1997; Vol. 489, p. 219. https://doi.org/10.1007/BFb0105678.
11. Share, G.H.; Murphy, R.J. Gamma Ray Spectroscopy in the Pre-HESSI Era. In Proceedings of the High Energy Solar Physics Workshop - Anticipating Hess!; Ramaty, R.; Mandzhavidze, N., Eds., 2000, Vol. 206, *Astronomical Society of the Pacific Conference Series*, p. 377.
12. Vilmer, N.; MacKinnon, A.L.; Trottet, G.; Barat, C. High energy particles accelerated during the large solar flare of 1990 May 24: X/γ-ray observations. A&A **2003**, *412*, 865–874. https://doi.org/10.1051/0004-6361:20031488.
13. Share, G.H.; Murphy, R.J. Gamma Radiation From Flare-Accelerated Particles Impacting the Sun. *Geophysical Monograph Series* **2006**, *165*, 177. https://doi.org/10.1029/165GM17.
14. Vilmer, N.; MacKinnon, A.L.; Hurford, G.J. Properties of Energetic Ions in the Solar Atmosphere from γ-Ray and Neutron Observations. Space Sci. Rev. **2011**, *159*, 167–224, [arXiv:astro-ph.SR/1110.2432]. https://doi.org/10.1007/s11214-010-9728-x.

15. Stecker, F.W. The Cosmic γ-Ray Spectrum from Secondary Particle Production in Cosmic-Ray Interactions. Ap&SS **1970**, *6*, 377–389. https://doi.org/10.1007/BF00653856.
16. Murphy, R.J.; Dermer, C.D.; Ramaty, R. High-Energy Processes in Solar Flares. ApJS **1987**, *63*, 721. https://doi.org/10.1086/191180.
17. Hurford, G.J.; Schwartz, R.A.; Krucker, S.; Lin, R.P.; Smith, D.M.; Vilmer, N. First Gamma-Ray Images of a Solar Flare. ApJ **2003**, *595*, L77–L80. https://doi.org/10.1086/378179.
18. Ramaty, R.; Mandzhavidze, N. High energy processes in solar flares. In Proceedings of the Cosmic Explosions: Tenth AstroPhysics Conference; Holt, S.S.; Zhang, W.W., Eds., 2000, Vol. 522, *American Institute of Physics Conference Series*, pp. 401–410. https://doi.org/10.1063/1.1291742.
19. Emslie, A.G.; Dennis, B.R.; Shih, A.Y.; Chamberlin, P.C.; Mewaldt, R.A.; Moore, C.S.; Share, G.H.; Vourlidas, A.; Welsch, B.T. Global Energetics of Thirty-eight Large Solar Eruptive Events. ApJ **2012**, *759*, 71, [arXiv:astro-ph.SR/1209.2654]. https://doi.org/10.1088/0004-637X/759/1/71.
20. Aschwanden, M.J.; Caspi, A.; Cohen, C.M.S.; Holman, G.; Jing, J.; Kretzschmar, M.; Kontar, E.P.; McTiernan, J.M.; Mewaldt, R.A.; O'Flannagain, A.; et al. Global Energetics of Solar Flares. V. Energy Closure in Flares and Coronal Mass Ejections. ApJ **2017**, *836*, 17, [arXiv:astro-ph.SR/1701.01176]. https://doi.org/10.3847/1538-4357/836/1/17.
21. Lin, R.P.; Dennis, B.R.; Hurford, G.J.; Smith, D.M.; Zehnder, A.; Harvey, P.R.; Curtis, D.W.; Pankow, D.; Turin, P.; Bester, M.; et al. The Reuven Ramaty High-Energy Solar Spectroscopic Imager (RHESSI). Sol. Phys. **2002**, *210*, 3–32. https://doi.org/10.1023/A:1022428818870.
22. Krucker, S.; Hurford, G.J.; Grimm, O.; Kögl, S.; Gröbelbauer, H.P.; Etesi, L.; Casadei, D.; Csillaghy, A.; Benz, A.O.; Arnold, N.G.; et al. The Spectrometer/Telescope for Imaging X-rays (STIX). A&A **2020**, *642*, A15. https://doi.org/10.1051/0004-6361/201937362.
23. Culhane, J.L.; Harra, L.K.; James, A.M.; Al-Janabi, K.; Bradley, L.J.; Chaudry, R.A.; Rees, K.; Tandy, J.A.; Thomas, P.; Whillock, M.C.R.; et al. The EUV Imaging Spectrometer for Hinode. Sol. Phys. **2007**, *243*, 19–61. https://doi.org/10.1007/s01007-007-0293-1.
24. SPICE Consortium.; Anderson, M.; Appourchaux, T.; Auchère, F.; Aznar Cuadrado, R.; Barbay, J.; Baudin, F.; Beardsley, S.; Bocchialini, K.; Borgo, B.; et al. The Solar Orbiter SPICE instrument. An extreme UV imaging spectrometer. A&A **2020**, *642*, A14, [arXiv:astro-ph.IM/1909.01183]. https://doi.org/10.1051/0004-6361/201935574.
25. Aschwanden, M.J.; Kontar, E.P.; Jeffrey, N.L.S. Global Energetics of Solar Flares. VIII. The Low-energy Cutoff. ApJ **2019**, *881*, 1, [arXiv:astro-ph.SR/1906.05835]. https://doi.org/10.3847/1538-4357/ab2cd4.
26. Drake, J.F.; Swisdak, M.; Che, H.; Shay, M.A. Electron acceleration from contracting magnetic islands during reconnection. Nature **2006**, *443*, 553–556. https://doi.org/10.1038/nature05116.
27. Arnold, H.; Drake, J.F.; Swisdak, M.; Guo, F.; Dahlin, J.T.; Chen, B.; Fleishman, G.; Glesener, L.; Kontar, E.; Phan, T.; et al. Electron Acceleration during Macroscale Magnetic Reconnection. Phys. Rev. Lett. **2021**, *126*, 135101, [arXiv:physics.plasm-ph/2011.01147]. https://doi.org/10.1103/PhysRevLett.126.135101.
28. Miller, J.A.; Cargill, P.J.; Emslie, A.G.; Holman, G.D.; Dennis, B.R.; LaRosa, T.N.; Winglee, R.M.; Benka, S.G.; Tsuneta, S. Critical issues for understanding particle acceleration in impulsive solar flares. J. Geophys. Res. **1997**, *102*, 14631–14660. https://doi.org/10.1029/97JA00976.
29. Petrosian, A.R.; Boulesteix, J.; Comte, G.; Kunth, D.; Lecoarer, E. An interferometric study of the blue compact dwarf galaxy IZW 18. A&A **1997**, *318*, 390–404, [arXiv:astro-ph/astro-ph/9612079].
30. Vlahos, L.; Anastasiadis, A.; Papaioannou, A.; Kouloumvakos, A.; Isliker, H. Sources of solar energetic particles. *Philosophical Transactions of the Royal Society of London Series A* **2019**, *377*, 20180095, [arXiv:astro-ph.HE/1903.08200]. https://doi.org/10.1098/rsta.2018.0095.
31. Vlahos, L.; Isliker, H. Particle acceleration and heating in a turbulent solar corona. *Plasma Physics and Controlled Fusion* **2019**, *61*, 014020, [arXiv:astro-ph.HE/1808.07136]. https://doi.org/10.1088/1361-6587/aadbe7.
32. Kiener, J.; Gros, M.; Tatischeff, V.; Weidenspointner, G. Properties of the energetic particle distributions during the October 28, 2003 solar flare from INTEGRAL/SPI observations. A&A **2006**, *445*, 725–733, [arXiv:astro-ph/astro-ph/0511091]. https://doi.org/10.1051/0004-6361:20053665.
33. Litvinenko, Y.E.; Craig, I.J.D. Flare Energy Release by Flux Pile-up Magnetic Reconnection in a Turbulent Current Sheet. ApJ **2000**, *544*, 1101–1107. https://doi.org/10.1086/317262.
34. Holman, G.D.; Benka, S.G. A Hybrid Thermal/Nonthermal Model for the Energetic Emissions from Solar Flares. ApJ **1992**, *400*, L79. https://doi.org/10.1086/186654.
35. Alexander, W.M.; Tanner, W.G.; McDonald, R.A.; Schaub, G.E.; Stephenson, S.L.; McDonnell, J.A.M.; Maag, C.R. The Status of Measurement Technologies Concerning Micrometer and Submicrometer Space Articulate Matter Capture, Recovery, Velocity, and Trajectory. In Proceedings of the Particle Capture, Recovery and Velocity/Trajectory Measurement Technologies; Zolensky, M.E., Ed., 1994, p. 11.
36. Dunphy, P.P.; Chupp, E.L.; Bertsch, D.L.; Schneid, E.J.; Gottesman, S.R.; Kanbach, G. Gamma-Rays and Neutrons as a Probe of Flare Proton Spectra: the Solar Flare of 11 June 1991. Sol. Phys. **1999**, *187*, 45–57. https://doi.org/10.1023/A:1005143603547.
37. Kocharov, L.G.; Lee, J.W.; Zirin, H.; Kovaltsov, G.A.; Usoskin, I.G.; Pyle, K.R.; Shea, M.A.; Smart, D.F. Neutron and electromagnetic emissions during the 1990 May 24 solar flare. Sol. Phys. **1994**, *155*, 149–170. https://doi.org/10.1007/BF00670736.
38. Kocharov, L.; Debrunner, H.; Kovaltsov, G.; Lockwood, J.; McConnell, M.; Nieminen, P.; Rank, G.; Ryan, J.; Schoenfelder, V. Deduced spectrum of interacting protons accelerated after the impulsive phase of the 15 June 1991 solar flare. A&A **1998**, *340*, 257–264.
39. Vilmer, N.; Krucker, S.; Trottet, G.; Lin, R.P. Hard X-ray and metric/decimetric spatially resolved observations of the 10 April 2002 solar flare. *Advances in Space Research* **2003**, *32*, 2509–2515. https://doi.org/10.1016/j.asr.2003.04.005.
40. Kanbach, G.; Bertsch, D.L.; Fichtel, C.E.; Hartman, R.C.; Hunter, S.D.; Kniffen, D.A.; Kwok, P.W.; Lin, Y.C.; Mattox, J.R.; Mayer-Hasselwander, H.A. Detection of a long-duration solar gamma-ray flare on June 11, 1991 with EGRET on COMPTON-GRO. A&AS **1993**, *97*, 349–353.

41. Ryan, J.M.; Lockwood, J.A.; Debrunner, H. Solar Energetic Particles. Space Sci. Rev. **2000**, *93*, 35–53. https://doi.org/10.1023/A:1026580008909.
42. Kontar, E.P.; Perez, J.E.; Harra, L.K.; Kuznetsov, A.A.; Emslie, A.G.; Jeffrey, N.L.S.; Bian, N.H.; Dennis, B.R. Turbulent Kinetic Energy in the Energy Balance of a Solar Flare. Phys. Rev. Lett. **2017**, *118*, 155101, [arXiv:astro-ph.SR/1703.02392]. https://doi.org/10.1103/PhysRevLett.118.155101.
43. Allred, J.C.; Hawley, S.L.; Abbett, W.P.; Carlsson, M. Radiative Hydrodynamic Models of the Optical and Ultraviolet Emission from Solar Flares. ApJ **2005**, *630*, 573–586, [arXiv:astro-ph/astro-ph/0507335]. https://doi.org/10.1086/431751.
44. Allred, J.C.; Kowalski, A.F.; Carlsson, M. A Unified Computational Model for Solar and Stellar Flares. ApJ **2015**, *809*, 104, [arXiv:astro-ph.SR/1507.04375]. https://doi.org/10.1088/0004-637X/809/1/104.
45. Allred, J.C.; Kerr, G.S.; Gordon Emslie, A. Solar Flare Heating with Turbulent Suppression of Thermal Conduction. ApJ **2022**, *931*, 60, [arXiv:astro-ph.SR/2204.11684]. https://doi.org/10.3847/1538-4357/ac69e8.
46. Kowalski, A.F.; Hawley, S.L.; Carlsson, M.; Allred, J.C.; Uitenbroek, H.; Osten, R.A.; Holman, G. New Insights into White-Light Flare Emission from Radiative-Hydrodynamic Modeling of a Chromospheric Condensation. Sol. Phys. **2015**, *290*, 3487–3523, [arXiv:astro-ph.SR/1503.07057]. https://doi.org/10.1007/s11207-015-0708-x.
47. Kowalski, A.F.; Allred, J.C.; Daw, A.; Cauzzi, G.; Carlsson, M. The Atmospheric Response to High Nonthermal Electron Beam Fluxes in Solar Flares. I. Modeling the Brightest NUV Footpoints in the X1 Solar Flare of 2014 March 29. ApJ **2017**, *836*, 12, [arXiv:astro-ph.SR/1609.07390]. https://doi.org/10.3847/1538-4357/836/1/12.
48. Rubio da Costa, F.; Kleint, L.; Petrosian, V.; Liu, W.; Allred, J.C. Data-driven Radiative Hydrodynamic Modeling of the 2014 March 29 X1.0 Solar Flare. ApJ **2016**, *827*, 38, [arXiv:astro-ph.SR/1603.04951]. https://doi.org/10.3847/0004-637X/827/1/38.
49. Kerr, G.S.; Fletcher, L.; Russell, A.J.B.; Allred, J.C. Simulations of the Mg II k and Ca II 8542 lines from an AlfvÉn Wave-heated Flare Chromosphere. ApJ **2016**, *827*, 101, [arXiv:astro-ph.SR/1605.05888]. https://doi.org/10.3847/0004-637X/827/2/101.
50. Kerr, G.S.; Carlsson, M.; Allred, J.C.; Young, P.R.; Daw, A.N. SI IV Resonance Line Emission during Solar Flares: Non-LTE, Nonequilibrium, Radiation Transfer Simulations. ApJ **2019**, *871*, 23, [arXiv:astro-ph.SR/1811.11075]. https://doi.org/10.3847/1538-4357/aaf46e.
51. Kerr, G.S.; Allred, J.C.; Polito, V. Solar Flare Arcade Modeling: Bridging the Gap from 1D to 3D Simulations of Optically Thin Radiation. ApJ **2020**, *900*, 18, [arXiv:astro-ph.SR/2007.13856]. https://doi.org/10.3847/1538-4357/abaa46.
52. Brown, S.A.; Fletcher, L.; Kerr, G.S.; Labrosse, N.; Kowalski, A.F.; De La Cruz Rodríguez, J. Modeling of the Hydrogen Lyman Lines in Solar Flares. ApJ **2018**, *862*, 59, [arXiv:astro-ph.SR/1807.03373]. https://doi.org/10.3847/1538-4357/aacc29.
53. Polito, V.; Testa, P.; Allred, J.; De Pontieu, B.; Carlsson, M.; Pereira, T.M.D.; Gošić, M.; Reale, F. Investigating the Response of Loop Plasma to Nanoflare Heating Using RADYN Simulations. ApJ **2018**, *856*, 178, [arXiv:astro-ph.SR/1804.05970]. https://doi.org/10.3847/1538-4357/aab49e.
54. Polito, V.; Testa, P.; De Pontieu, B. Can the Superposition of Evaporative Flows Explain Broad Fe XXI Profiles during Solar Flares? ApJ **2019**, *879*, L17. https://doi.org/10.3847/2041-8213/ab290b.
55. Zhu, Y.; Kowalski, A.F.; Tian, H.; Uitenbroek, H.; Carlsson, M.; Allred, J.C. Modeling Mg II h, k and Triplet Lines at Solar Flare Ribbons. ApJ **2019**, *879*, 19, [arXiv:astro-ph.SR/1904.12285]. https://doi.org/10.3847/1538-4357/ab2238.
56. Reep, J.W.; Polito, V.; Warren, H.P.; Crump, N.A. The Duration of Energy Deposition on Unresolved Flaring Loops in the Solar Corona. ApJ **2018**, *856*, 149, [arXiv:astro-ph.SR/1802.08884]. https://doi.org/10.3847/1538-4357/aab273.
57. Reep, J.W.; Russell, A.J.B. Alfvénic Wave Heating of the Upper Chromosphere in Flares. ApJ **2016**, *818*, L20, [arXiv:astro-ph.SR/1601.01969]. https://doi.org/10.3847/2041-8205/818/1/L20.
58. Reep, J.W.; Russell, A.J.B.; Tarr, L.A.; Leake, J.E. A Hydrodynamic Model of Alfvénic Wave Heating in a Coronal Loop and Its Chromospheric Footpoints. ApJ **2018**, *853*, 101, [arXiv:astro-ph.SR/1712.06171]. https://doi.org/10.3847/1538-4357/aaa2fe.
59. Reep, J.W.; Bradshaw, S.J.; Crump, N.A.; Warren, H.P. Efficient Calculation of Non-local Thermodynamic Equilibrium Effects in Multithreaded Hydrodynamic Simulations of Solar Flares. ApJ **2019**, *871*, 18, [arXiv:astro-ph.SR/1806.09574]. https://doi.org/10.3847/1538-4357/aaf580.
60. Cheung, M.C.M.; Rempel, M.; Chintzoglou, G.; Chen, F.; Testa, P.; Martínez-Sykora, J.; Sainz Dalda, A.; DeRosa, M.L.; Malanushenko, A.; Hansteen, V.; et al. A comprehensive three-dimensional radiative magnetohydrodynamic simulation of a solar flare. *Nature Astronomy* **2019**, *3*, 160–166. https://doi.org/10.1038/s41550-018-0629-3.
61. Hurford, G.J.; Krucker, S.; Lin, R.P.; Schwartz, R.A.; Share, G.H.; Smith, D.M. Gamma-Ray Imaging of the 2003 October/November Solar Flares. ApJ **2006**, *644*, L93–L96. https://doi.org/10.1086/505329.
62. del Zanna, G.; Schmieder, B.; Mason, H.; Berlicki, A.; Bradshaw, S. The Gradual Phase of the X17 Flare on October 28, 2003. Sol. Phys. **2006**, *239*, 173–191. https://doi.org/10.1007/s11207-006-0184-4.
63. Milligan, R.O.; Dennis, B.R. Velocity Characteristics of Evaporated Plasma Using Hinode/EUV Imaging Spectrometer. ApJ **2009**, *699*, 968–975, [arXiv:astro-ph.SR/0905.1669]. https://doi.org/10.1088/0004-637X/699/2/968.
64. Milligan, R.O. Spatially Resolved Nonthermal Line Broadening during the Impulsive Phase of a Solar Flare. ApJ **2011**, *740*, 70, [arXiv:astro-ph.SR/1202.1737]. https://doi.org/10.1088/0004-637X/740/2/70.
65. Nakariakov, V.M.; Melnikov, V.F. Quasi-Periodic Pulsations in Solar Flares. Space Sci. Rev. **2009**, *149*, 119–151. https://doi.org/10.1007/s11214-009-9536-3.
66. McLaughlin, J.A.; Nakariakov, V.M.; Dominique, M.; Jelínek, P.; Takasao, S. Modelling Quasi-Periodic Pulsations in Solar and Stellar Flares. Space Sci. Rev. **2018**, *214*, 45, [arXiv:astro-ph.SR/1802.04180]. https://doi.org/10.1007/s11214-018-0478-5.

67. Zimovets, I.V.; McLaughlin, J.A.; Srivastava, A.K.; Kolotkov, D.Y.; Kuznetsov, A.A.; Kupriyanova, E.G.; Cho, I.H.; Inglis, A.R.; Reale, F.; Pascoe, D.J.; et al. Quasi-Periodic Pulsations in Solar and Stellar Flares: A Review of Underpinning Physical Mechanisms and Their Predicted Observational Signatures. Space Sci. Rev. **2021**, *217*, 66. https://doi.org/10.1007/s11214-021-00840-9.
68. Nakariakov, V.M.; Kolotkov, D.Y.; Kupriyanova, E.G.; Mehta, T.; Pugh, C.E.; Lee, D.H.; Broomhall, A.M. Non-stationary quasi-periodic pulsations in solar and stellar flares. *Plasma Physics and Controlled Fusion* **2019**, *61*, 014024. https://doi.org/10.1088/1361-6587/aad97c.
69. Hayes, L.A.; Inglis, A.R.; Christe, S.; Dennis, B.; Gallagher, P.T. Statistical Study of GOES X-Ray Quasi-periodic Pulsations in Solar Flares. ApJ **2020**, *895*, 50, [arXiv:astro-ph.SR/2004.11775]. https://doi.org/10.3847/1538-4357/ab8d40.
70. Emslie, A.G.; Sturrock, P.A. Temperature minimum heating in solar flares by resistive dissipation of Alfvén waves. Sol. Phys. **1982**, *80*, 99–112. https://doi.org/10.1007/BF00153426.
71. Fletcher, L.; Hudson, H.S. Impulsive Phase Flare Energy Transport by Large-Scale Alfvén Waves and the Electron Acceleration Problem. ApJ **2008**, *675*, 1645–1655, [arXiv:astro-ph/0712.3452]. https://doi.org/10.1086/527044.
72. Russell, A.J.B.; Fletcher, L. Propagation of Alfvénic Waves from Corona to Chromosphere and Consequences for Solar Flares. ApJ **2013**, *765*, 81, [arXiv:astro-ph.SR/1302.2458]. https://doi.org/10.1088/0004-637X/765/2/81.
73. Cheung, M.C.M.; Martínez-Sykora, J.; Testa, P.; De Pontieu, B.; Chintzoglou, G.; Rempel, M.; Polito, V.; Kerr, G.S.; Reeves, K.K.; Fletcher, L.; et al. Probing the Physics of the Solar Atmosphere with the Multi-slit Solar Explorer (MUSE). II. Flares and Eruptions. ApJ **2022**, *926*, 53, [arXiv:astro-ph.SR/2106.15591]. https://doi.org/10.3847/1538-4357/ac4223.
74. Laming, J.M. The FIP and Inverse-FIP Effects in Solar Flares. ApJ **2021**, *909*, 17, [arXiv:astro-ph.SR/2101.03038]. https://doi.org/10.3847/1538-4357/abd9c3.
75. Malandraki, O.E.; Crosby, N.B. Solar Energetic Particles and Space Weather: Science and Applications. In Proceedings of the Solar Particle Radiation Storms Forecasting and Analysis; Malandraki, O.E.; Crosby, N.B., Eds., 2018, Vol. 444, *Astrophysics and Space Science Library*, pp. 1–26. https://doi.org/10.1007/978-3-319-60051-2_1.
76. McComas, D.J.; Christian, E.R.; Cohen, C.M.S.; Cummings, A.C.; Davis, A.J.; Desai, M.I.; Giacalone, J.; Hill, M.E.; Joyce, C.J.; Krimigis, S.M.; et al. Probing the energetic particle environment near the Sun. Nature **2019**, *576*, 223–227. https://doi.org/10.1038/s41586-019-1811-1.
77. Gómez-Herrero, R.; Pacheco, D.; Kollhoff, A.; Espinosa Lara, F.; Freiherr von Forstner, J.L.; Dresing, N.; Lario, D.; Balmaceda, L.; Krupar, V.; Malandraki, O.E.; et al. First near-relativistic solar electron events observed by EPD onboard Solar Orbiter. A&A **2021**, *656*, L3. https://doi.org/10.1051/0004-6361/202039883.
78. Pick, M.; Vilmer, N. Sixty-five years of solar radioastronomy: flares, coronal mass ejections and Sun Earth connection. A&A Rev. **2008**, *16*, 1–153. https://doi.org/10.1007/s00159-008-0013-x.
79. Reid, H.A.S.; Ratcliffe, H. A review of solar type III radio bursts. *Research in Astronomy and Astrophysics* **2014**, *14*, 773–804, [arXiv:astro-ph.SR/1404.6117]. https://doi.org/10.1088/1674-4527/14/7/003.
80. Masson, S.; Antiochos, S.K.; DeVore, C.R. Escape of Flare-accelerated Particles in Solar Eruptive Events. ApJ **2019**, *884*, 143, [arXiv:astro-ph.SR/1909.13578]. https://doi.org/10.3847/1538-4357/ab4515.
81. Reid, H.A.S. A review of recent type III imaging spectroscopy. *Frontiers in Astronomy and Space Sciences* **2020**, *7*, 56. https://doi.org/10.3389/fspas.2020.00056.
82. Steinberg, J.L.; Aubier-Giraud, M.; Leblanc, Y.; Boischot, A. Coronal Scattering, Absorption and Refraction of Solar Radiobursts. A&A **1971**, *10*, 362.
83. Kontar, E.P.; Chen, X.; Chrysaphi, N.; Jeffrey, N.L.S.; Emslie, A.G.; Krupar, V.; Maksimovic, M.; Gordovskyy, M.; Browning, P.K. Anisotropic Radio-wave Scattering and the Interpretation of Solar Radio Emission Observations. ApJ **2019**, *884*, 122, [arXiv:astro-ph.SR/1909.00340]. https://doi.org/10.3847/1538-4357/ab40bb.
84. Saint-Hilaire, P.; Krucker, S.; Christe, S.; Lin, R.P. The X-ray Detectability of Electron Beams Escaping from the Sun. ApJ **2009**, *696*, 941–952, [arXiv:astro-ph.SR/1111.4250]. https://doi.org/10.1088/0004-637X/696/1/941.
85. Longcope, D.W.; Guidoni, S.E.; Linton, M.G. Gas-dynamic Shock Heating of Post-flare Loops Due to Retraction Following Localized, Impulsive Reconnection. ApJ **2009**, *690*, L18–L22, [arXiv:astro-ph/0810.3661]. https://doi.org/10.1088/0004-637X/690/1/L18.
86. Reeves, K.K.; McCauley, P.I.; Tian, H. Direct Observations of Magnetic Reconnection Outflow and CME Triggering in a Small Erupting Solar Prominence. ApJ **2015**, *807*, 7, [arXiv:astro-ph.SR/1505.07307]. https://doi.org/10.1088/0004-637X/807/1/7.
87. Zharkova, V.V.; Arzner, K.; Benz, A.O.; Browning, P.; Dauphin, C.; Emslie, A.G.; Fletcher, L.; Kontar, E.P.; Mann, G.; Onofri, M.; et al. Recent Advances in Understanding Particle Acceleration Processes in Solar Flares. Space Sci. Rev. **2011**, *159*, 357–420, [arXiv:astro-ph.SR/1110.2359]. https://doi.org/10.1007/s11214-011-9803-y.
88. Moore, R.L.; Sterling, A.C.; Hudson, H.S.; Lemen, J.R. Onset of the Magnetic Explosion in Solar Flares and Coronal Mass Ejections. ApJ **2001**, *552*, 833–848. https://doi.org/10.1086/320559.
89. Lin, J.; Forbes, T.G. Effects of reconnection on the coronal mass ejection process. J. Geophys. Res. **2000**, *105*, 2375–2392. https://doi.org/10.1029/1999JA900477.
90. Antiochos, S.K.; DeVore, C.R.; Klimchuk, J.A. A Model for Solar Coronal Mass Ejections. ApJ **1999**, *510*, 485–493, [arXiv:astro-ph/astro-ph/9807220]. https://doi.org/10.1086/306563.
91. Török, T.; Kliem, B. Confined and Ejective Eruptions of Kink-unstable Flux Ropes. ApJ **2005**, *630*, L97–L100, [arXiv:astro-ph/astro-ph/0507662]. https://doi.org/10.1086/462412.
92. Wyper, P.F.; DeVore, C.R.; Antiochos, S.K. A Breakout Model for Solar Coronal Jets with Filaments. ApJ **2018**, *852*, 98, [arXiv:astro-ph.SR/1712.00134]. https://doi.org/10.3847/1538-4357/aa9ffc.

93. Pariat, E.; Dalmasse, K.; DeVore, C.R.; Antiochos, S.K.; Karpen, J.T. A model for straight and helical solar jets. II. Parametric study of the plasma beta. A&A **2016**, *596*, A36, [arXiv:astro-ph.SR/1609.08825]. https://doi.org/10.1051/0004-6361/201629109.
94. Pariat, E.; Dalmasse, K.; DeVore, C.R.; Antiochos, S.K.; Karpen, J.T. Model for straight and helical solar jets. I. Parametric studies of the magnetic field geometry. A&A **2015**, *573*, A130. https://doi.org/10.1051/0004-6361/201424209.
95. Wyper, P.F.; DeVore, C.R.; Karpen, J.T.; Antiochos, S.K.; Yeates, A.R. A Model for Coronal Hole Bright Points and Jets Due to Moving Magnetic Elements. ApJ **2018**, *864*, 165, [arXiv:astro-ph.SR/1808.03688]. https://doi.org/10.3847/1538-4357/aad9f7.
96. Parnell, C.E.; De Moortel, I. A contemporary view of coronal heating. *Philosophical Transactions of the Royal Society of London Series A* **2012**, *370*, 3217–3240, [arXiv:astro-ph.SR/1206.6097]. https://doi.org/10.1098/rsta.2012.0113.
97. Klimchuk, J.A. On Solving the Coronal Heating Problem. Sol. Phys. **2006**, *234*, 41–77, [arXiv:astro-ph/astro-ph/0511841]. https://doi.org/10.1007/s11207-006-0055-z.
98. Klimchuk, J.A. Key aspects of coronal heating. *Philosophical Transactions of the Royal Society of London Series A* **2015**, *373*, 20140256–20140256, [arXiv:astro-ph.SR/1410.5660]. https://doi.org/10.1098/rsta.2014.0256.
99. Klimchuk, J.A.; Luna, M. The Role of Asymmetries in Thermal Nonequilibrium. ApJ **2019**, *884*, 68, [arXiv:astro-ph.SR/1905.09767]. https://doi.org/10.3847/1538-4357/ab41f4.
100. Viall, N.M.; Borovsky, J.E. Nine Outstanding Questions of Solar Wind Physics. *Journal of Geophysical Research (Space Physics)* **2020**, *125*, e26005. https://doi.org/10.1029/2018JA026005.
101. Hannah, I.G.; Hudson, H.S.; Battaglia, M.; Christe, S.; Kašparová, J.; Krucker, S.; Kundu, M.R.; Veronig, A. Microflares and the Statistics of X-ray Flares. Space Sci. Rev. **2011**, *159*, 263–300, [arXiv:astro-ph.SR/1108.6203]. https://doi.org/10.1007/s11214-010-9705-4.
102. Testa, P.; De Pontieu, B.; Allred, J.; Carlsson, M.; Reale, F.; Daw, A.; Hansteen, V.; Martinez-Sykora, J.; Liu, W.; DeLuca, E.E.; et al. Evidence of nonthermal particles in coronal loops heated impulsively by nanoflares. *Science* **2014**, *346*, 1255724, [arXiv:astro-ph.SR/1410.6130]. https://doi.org/10.1126/science.1255724.
103. Dudík, J.; Dzifčáková, E.; Meyer-Vernet, N.; Del Zanna, G.; Young, P.R.; Giunta, A.; Sylwester, B.; Sylwester, J.; Oka, M.; Mason, H.E.; et al. Nonequilibrium Processes in the Solar Corona, Transition Region, Flares, and Solar Wind (Invited Review). Sol. Phys. **2017**, *292*, 100, [arXiv:astro-ph.SR/1706.03396]. https://doi.org/10.1007/s11207-017-1125-0.
104. Benz, A.O.; Grigis, P.C. Microflares and hot component in solar active regions. Sol. Phys. **2002**, *210*, 431–444, [arXiv:astro-ph/astro-ph/0210024]. https://doi.org/10.1023/A:1022496515506.
105. Krucker, S.; Christe, S.; Lin, R.P.; Hurford, G.J.; Schwartz, R.A. Hard X-ray Microflares down to 3 keV. Sol. Phys. **2002**, *210*, 445–456. https://doi.org/10.1023/A:1022404512780.
106. Christe, S.; Hannah, I.G.; Krucker, S.; McTiernan, J.; Lin, R.P. RHESSI Microflare Statistics. I. Flare-Finding and Frequency Distributions. ApJ **2008**, *677*, 1385–1394. https://doi.org/10.1086/529011.
107. Warmuth, A.; Mann, G. Constraints on energy release in solar flares from RHESSI and GOES X-ray observations. II. Energetics and energy partition. A&A **2016**, *588*, A116. https://doi.org/10.1051/0004-6361/201527475.
108. Hannah, I.G.; Christe, S.; Krucker, S.; Hurford, G.J.; Hudson, H.S.; Lin, R.P. RHESSI Microflare Statistics. II. X-Ray Imaging, Spectroscopy, and Energy Distributions. ApJ **2008**, *677*, 704–718, [arXiv:astro-ph/0712.2544]. https://doi.org/10.1086/529012.
109. Battaglia, A.F.; Saqri, J.; Massa, P.; Perracchione, E.; Dickson, E.C.M.; Xiao, H.; Veronig, A.M.; Warmuth, A.; Battaglia, M.; Hurford, G.J.; et al. STIX X-ray microflare observations during the Solar Orbiter commissioning phase. A&A **2021**, *656*, A4, [arXiv:astro-ph.SR/2106.10058]. https://doi.org/10.1051/0004-6361/202140524.
110. Saqri, J.; Veronig, A.M.; Warmuth, A.; Dickson, E.C.M.; Battaglia, A.F.; Podladchikova, T.; Xiao, H.; Battaglia, M.; Hurford, G.J.; Krucker, S. Multi-instrument STIX microflare study. A&A **2022**, *659*, A52, [arXiv:astro-ph.SR/2201.00712]. https://doi.org/10.1051/0004-6361/202142373.
111. Glesener, L.; Krucker, S.; Duncan, J.; Hannah, I.G.; Grefenstette, B.W.; Chen, B.; Smith, D.M.; White, S.M.; Hudson, H. Accelerated Electrons Observed Down to <7 keV in a NuSTAR Solar Microflare. ApJ **2020**, *891*, L34, [arXiv:astro-ph.SR/2003.12864]. https://doi.org/10.3847/2041-8213/ab7341.
112. Cooper, K.; Hannah, I.G.; Grefenstette, B.W.; Glesener, L.; Krucker, S.; Hudson, H.S.; White, S.M.; Smith, D.M.; Duncan, J. NuSTAR observations of a repeatedly microflaring active region. MNRAS **2021**, *507*, 3936–3951, [arXiv:astro-ph.SR/2109.00263]. https://doi.org/10.1093/mnras/stab2283.
113. Duncan, J.; Glesener, L.; Grefenstette, B.W.; Vievering, J.; Hannah, I.G.; Smith, D.M.; Krucker, S.; White, S.M.; Hudson, H. NuSTAR Observation of Energy Release in 11 Solar Microflares. ApJ **2021**, *908*, 29, [arXiv:astro-ph.SR/2011.06651]. https://doi.org/10.3847/1538-4357/abca3d.
114. Warmuth, A.; Mann, G. Thermal-nonthermal energy partition in solar flares derived from X-ray, EUV, and bolometric observations. Discussion of recent studies. A&A **2020**, *644*, A172, [arXiv:astro-ph.SR/2011.04442]. https://doi.org/10.1051/0004-6361/202039529.
115. Schmelz, J.T.; Kashyap, V.L.; Saar, S.H.; Dennis, B.R.; Grigis, P.C.; Lin, L.; De Luca, E.E.; Holman, G.D.; Golub, L.; Weber, M.A. Some Like It Hot: Coronal Heating Observations from Hinode X-ray Telescope and RHESSI. ApJ **2009**, *704*, 863–869. https://doi.org/10.1088/0004-637X/704/1/863.
116. Brosius, J.W.; Daw, A.N.; Rabin, D.M. Pervasive Faint Fe XIX Emission from a Solar Active Region Observed with EUNIS-13: Evidence for Nanoflare Heating. ApJ **2014**, *790*, 112. https://doi.org/10.1088/0004-637X/790/2/112.
117. Caspi, A.; Woods, T.N.; Warren, H.P. New Observations of the Solar 0.5-5 keV Soft X-Ray Spectrum. ApJ **2015**, *802*, L2, [arXiv:astro-ph.SR/1502.01725]. https://doi.org/10.1088/2041-8205/802/1/L2.

118. Del Zanna, G.; Andretta, V.; Cargill, P.J.; Corso, A.J.; Daw, A.N.; Golub, L.; Klimchuk, J.A.; Mason, H.E. High resolution soft X-ray spectroscopy and the quest for the hot (5-10 MK) plasma in solar active regions. *Frontiers in Astronomy and Space Sciences* **2021**, *8*, 33, [arXiv:astro-ph.SR/2103.06156]. https://doi.org/10.3389/fspas.2021.638489.
119. Bradshaw, S.J.; Klimchuk, J.A. What Dominates the Coronal Emission Spectrum During the Cycle of Impulsive Heating and Cooling? ApJS **2011**, *194*, 26. https://doi.org/10.1088/0067-0049/194/2/26.
120. Golub, L.; Hartquist, T.W.; Quillen, A.C. Comments on the Observability of Coronal Variations. Sol. Phys. **1989**, *122*, 245–261. https://doi.org/10.1007/BF00912995.
121. Reale, F.; Orlando, S. Nonequilibrium of Ionization and the Detection of Hot Plasma in Nanoflare-heated Coronal Loops. ApJ **2008**, *684*, 715–724, [arXiv:astro-ph/0805.3512]. https://doi.org/10.1086/590338.
122. Lörinčík, J.; Dudík, J.; del Zanna, G.; Dzifčáková, E.; Mason, H.E. Plasma Diagnostics from Active Region and Quiet-Sun Spectra Observed by Hinode/EIS: Quantifying the Departures from a Maxwellian Distribution. ApJ **2020**, *893*, 34. https://doi.org/10.3847/1538-4357/ab8010.
123. Dzifčáková, E.; Dudík, J.; Zemanová, A.; Lörinčík, J.; Karlický, M. KAPPA: A Package for the Synthesis of Optically Thin Spectra for the Non-Maxwellian κ-distributions. II. Major Update to Compatibility with CHIANTI Version 10. ApJS **2021**, *257*, 62. https://doi.org/10.3847/1538-4365/ac2aa7.
124. Del Zanna, G.; Polito, V.; Dudík, J.; Testa, P.; Mason, H.E.; Dzifčáková, E. Diagnostics of Non-Maxwellian Electron Distributions in Solar Active Regions from Fe XII Lines Observed by the Hinode Extreme Ultraviolet Imaging Spectrometer and Interface Region Imaging Spectrograph. ApJ **2022**, *930*, 61. https://doi.org/10.3847/1538-4357/ac6174.
125. Ishikawa, S.n.; Glesener, L.; Krucker, S.; Christe, S.; Buitrago-Casas, J.C.; Narukage, N.; Vievering, J. Detection of nanoflare-heated plasma in the solar corona by the FOXSI-2 sounding rocket. *Nature Astronomy* **2017**, *1*, 771–774. https://doi.org/10.1038/s41550-017-0269-z.
126. Moore, C.S.; Caspi, A.; Woods, T.N.; Chamberlin, P.C.; Dennis, B.R.; Jones, A.R.; Mason, J.P.; Schwartz, R.A.; Tolbert, A.K. The Instruments and Capabilities of the Miniature X-Ray Solar Spectrometer (MinXSS) CubeSats. Sol. Phys. **2018**, *293*, 21, [arXiv:astro-ph.SR/1801.01261]. https://doi.org/10.1007/s11207-018-1243-3.
127. Marsh, A.J.; Smith, D.M.; Glesener, L.; Klimchuk, J.A.; Bradshaw, S.J.; Vievering, J.; Hannah, I.G.; Christe, S.; Ishikawa, S.n.; Krucker, S. Hard X-Ray Constraints on Small-scale Coronal Heating Events. ApJ **2018**, *864*, 5, [arXiv:astro-ph.SR/1808.02630]. https://doi.org/10.3847/1538-4357/aad380.
128. Mandrini, C.H.; Démoulin, P.; Klimchuk, J.A. Magnetic Field and Plasma Scaling Laws: Their Implications for Coronal Heating Models. ApJ **2000**, *530*, 999–1015. https://doi.org/10.1086/308398.
129. Cranmer, S.R.; Winebarger, A.R. The Properties of the Solar Corona and Its Connection to the Solar Wind. ARA&A **2019**, *57*, 157–187, [arXiv:astro-ph.SR/1811.00461]. https://doi.org/10.1146/annurev-astro-091918-104416.
130. Brooks, D.H.; Warren, H.P.; Landi, E. Measurements of Coronal Magnetic Field Strengths in Solar Active Region Loops. ApJ **2021**, *915*, L24, [arXiv:astro-ph.SR/2106.10884]. https://doi.org/10.3847/2041-8213/ac0c84.
131. Hurford, G.J. X-ray imaging with collimators, masks and grids. *ISSI Scientific Reports Series* **2010**, *9*, 223–234.
132. Piana, M.; Emslie, A.; Massone, A.M.; Dennis, B.R. *Hard X-ray Imaging of Solar Flares*; Springer-Verlag: Berlin, 2022.
133. Massa, P.; Hurford, G.J.; Volpara, A.; Kuhar, M.; Battaglia, A.F.; Xiao, H.; Casadei, D.; Perracchione, E.; Garbarino, S.; Guastavino, S.; et al. STIX imaging I – Concept. *arXiv e-prints* **2023**, p. arXiv:2303.02485, [arXiv:astro-ph.IM/2303.02485]. https://doi.org/10.48550/arXiv.2303.02485.
134. Krucker, S.; Christe, S.; Glesener, L.; Ishikawa, S.n.; Ramsey, B.; Takahashi, T.; Watanabe, S.; Saito, S.; Gubarev, M.; Kilaru, K.; et al. First Images from the Focusing Optics X-Ray Solar Imager. ApJ **2014**, *793*, L32. https://doi.org/10.1088/2041-8205/793/2/L32.
135. Christe, S.; Glesener, L.; Buitrago-Casas, C.; Ishikawa, S.N.; Ramsey, B.; Gubarev, M.; Kilaru, K.; Kolodziejczak, J.J.; Watanabe, S.; Takahashi, T.; et al. FOXSI-2: Upgrades of the Focusing Optics X-ray Solar Imager for its Second Flight. *Journal of Astronomical Instrumentation* **2016**, *5*, 1640005–625. https://doi.org/10.1142/S2251171716400055.
136. Glesener, L.; Krucker, S.; Christe, S.; Ishikawa, S.n.; Buitrago-Casas, J.C.; Ramsey, B.; Gubarev, M.; Takahashi, T.; Watanabe, S.; Takeda, S.; et al. The FOXSI solar sounding rocket campaigns. In Proceedings of the Space Telescopes and Instrumentation 2016: Ultraviolet to Gamma Ray; den Herder, J.W.A.; Takahashi, T.; Bautz, M., Eds., 2016, Vol. 9905, *Society of Photo-Optical Instrumentation Engineers (SPIE) Conference Series*, p. 99050E. https://doi.org/10.1117/12.2232262.
137. Musset, S.; Buitrago-Casas, J.C.; Glesener, L.; Bongiorno, S.; Courtade, S.; Athiray, P.S.; Vievering, J.; Ishikawa, S.n.; Narukage, N.; Furukawa, K.; et al. Ghost-ray reduction and early results from the third FOXSI sounding rocket flight. In Proceedings of the UV, X-Ray, and Gamma-Ray Space Instrumentation for Astronomy XXI, 2019, Vol. 11118, *Society of Photo-Optical Instrumentation Engineers (SPIE) Conference Series*, p. 1111812. https://doi.org/10.1117/12.2530029.
138. Christe, S.D.; Shih, A.; Rodriguez, M.; Cramer, A.; Gregory, K.; Edgerton, M.; Gaskin, J.; Wilson-Hodge, C.; Apple, J.; Stevenson Chavis, K.; et al. The high energy replicated optics to explore the sun mission: a hard x-ray balloon-borne telescope. In Proceedings of the Solar Physics and Space Weather Instrumentation V; Fineschi, S.; Fennelly, J., Eds., 2013, Vol. 8862, *Society of Photo-Optical Instrumentation Engineers (SPIE) Conference Series*, p. 886206. https://doi.org/10.1117/12.2024323.
139. Christe, S.; Shih, A.Y.; Rodriguez, M.; Cramer, A.; Gregory, K.; Gaskin, J.; Chavis, K.; Smith, L.; HOPE/HEROES Team. The High Energy Replicated Optics to Explore the Sun (HEROES). In Proceedings of the AAS/Solar Physics Division Abstracts #44, 2013, Vol. 44, *AAS/Solar Physics Division Meeting*, p. 100.76.
140. Del Zanna, G.; Mason, H.E. Solar UV and X-ray spectral diagnostics. *Living Reviews in Solar Physics* **2018**, *15*, 5, [arXiv:astro-ph.SR/1809.01618]. https://doi.org/10.1007/s41116-018-0015-3.

141. Landi, E.; Hutton, R.; Brage, T.; Li, W. Hinode/EIS Measurements of Active-region Magnetic Fields. ApJ **2020**, *904*, 87, [arXiv:astro-ph.SR/2008.03532]. https://doi.org/10.3847/1538-4357/abbf54.
142. Dudík, J.; Del Zanna, G.; Mason, H.E.; Dzifčáková, E. Signatures of the non-Maxwellian κ-distributions in optically thin line spectra. I. Theory and synthetic Fe IX-XIII spectra. A&A **2014**, *570*, A124, [arXiv:astro-ph.SR/1408.0950]. https://doi.org/10.1051/0004-6361/201424124.
143. Dudík, J.; Mackovjak, Š.; Dzifčáková, E.; Del Zanna, G.; Williams, D.R.; Karlický, M.; Mason, H.E.; Lörinčík, J.; Kotrč, P.; Fárník, F.; et al. Imaging and Spectroscopic Observations of a Transient Coronal Loop: Evidence for the Non-Maxwellian K Distributions. ApJ **2015**, *807*, 123, [arXiv:astro-ph.SR/1505.04333]. https://doi.org/10.1088/0004-637X/807/2/123.
144. De Pontieu, B.; Martínez-Sykora, J.; Testa, P.; Winebarger, A.R.; Daw, A.; Hansteen, V.; Cheung, M.C.M.; Antolin, P. The Multi-slit Approach to Coronal Spectroscopy with the Multi-slit Solar Explorer (MUSE). ApJ **2020**, *888*, 3, [arXiv:astro-ph.IM/1909.08818]. https://doi.org/10.3847/1538-4357/ab5b03.
145. Matthews, S.A.; Reid, H.A.S.; Baker, D.; Bloomfield, D.S.; Browning, P.K.; Calcines, A.; Del Zanna, G.; Erdelyi, R.; Fletcher, L.; Hannah, I.G.; et al. The high-energy Sun - probing the origins of particle acceleration on our nearest star. *Experimental Astronomy* **2022**, *54*, 335–360. https://doi.org/10.1007/s10686-021-09798-6.